Available online at www.CivileJournal.org

Civil Engineering Journal

(E-ISSN: 2476-3055; ISSN: 2676-6957)

Vol. 11, No. 06, June, 2025

Predictive Modeling of CSH Formation in Cement Materials Based on SEM and EDS Analysis

Alexey N. Beskopylny [1*], Mohammad Hematibahar [2, 3], Makhmud Kharun [4], Sergei A. Stel'makh [5], Evgenii M. Shcherban' [6], Oxana Ananova [7]

[1] *Department of Transport Systems, Don State Technical University, 344003 Rostov-on-Don, Russia.*

[2] *Department of Architecture, Restoration and Design, RUDN University, 117198 Moscow, Russia.*

[3] *ANO "SAFAS", 3 Ordzhonikidze Ulitsa, 115419, Moscow, Russia.*

[4] *Department of Reinforced Concrete and Stone Structures, Moscow State University of Civil Engineering, 129337, Moscow, Russia.*

[5] *Department of Unique Buildings and Constructions Engineering, Don State Technical University, 344003 Rostov-on-Don, Russia*

[6] *Department of Engineering Geometry and Computer Graphics, Don State Technical University, 344003 Rostov-on-Don, Russia.*

[7] *Department of Marketing and Engineering Economics, Don State Technical University, 344003 Rostov-on-Don, Russia.*

Received 06 March 2025; Revised 18 May 2025; Accepted 22 May 2025; Published 01 June 2025

Abstract

Calcium silicate hydrate (CSH) formation is a fundamental process required to enhance the density, strength, and durability of cementitious materials. However, there is a gap in the research on the structural, physical, and chemical transformations of CSH. The objectives of this study are to develop a predictive model of CSH formation in cementitious materials and evaluate the effects of gelatin powder (GP), silica fume (MS), ground coffee (SCG), and peanut shell (PS) on CSH formation. Scanning Electron Microscopy (SEM) and Energy Dispersive X-Ray Spectroscopy (EDS) apply to the study of the composite cementitious materials. A multiple linear regression model is proposed to predict the changes of key elements, which improved the qualitative and quantitative understanding of the hydration mechanisms. The results show that GP significantly accelerates CSH formation by increasing the calcium and oxygen contents, while MS enhances pozzolanic activity by increasing the availability of silicon, resulting in structural densification. SCG contributes to the increase of carbon and oxygen by acting as a filler, while PS has minimal effect on hydration or crystallization. A regression model relating cement mix design proportions and CSH shows strong correlations between admixtures and chemical changes, particularly for calcium (R^2=0.988) and silica (R^2=0.985). To fill the existing research gaps, this study goes beyond previous studies, which primarily focused on individual aspects of CSH formation without considering the convergence of structural and chemical analysis.

Keywords: CSH; SEM; EDS; Hydration Process; Regression Model; Pozzolanic Reaction.

1. Introduction

Calcium silicate hydrate (CSH) is formed by the reaction of C3S or C2S with water. The most visible CSH is the crystalline material on the cement matrix. Even using X-ray diffraction, CSH cannot be detected. The composition of CSH stoichiometrically contains approximately as much SiO_2 as CaO plus some water [1].

* Corresponding author: besk-an@yandex.ru

http://dx.doi.org/10.28991/CEJ-2025-011-06-017

Microsilica (MS) and silica fume (SF) cause two effects when mixed with the cement matrix. The first is a chemical effect resulting from the formation of C-S-H gel when silica is added to the pozzolanic reaction of cement with calcium hydroxide (CH). Second, MS or SF can fill the spaces between cement and aggregates to form a composite material. In addition, hydrated cement paste increases the compressive strength of the cement matrix [2, 3]. According to the researchers, normal hydration of cement can form CH and C-S-H, and CH decreases the strength of cement and concrete matrix, while C-S-H can increase the strength of cement by mixing Nano-SiO_2 with CH. From another point of view, when C-S-H is formed in concrete and cement matrix, the aggregate-cement matrix is also strengthened, and this improves the compressive and flexural strength [4–7]. Some experiments, such as energy dispersive spectroscopy (EDS) and scanning electron microscopy (SEM), can partially clarify the effect of MS or SF on the formation of CSH. X-ray diffraction (XRD) and test results show that when SF or MS is mixed with concrete, the amount of un-hydrated cement phase decreases with the increase in MS or SF content. Moreover, when MS or SF is added to cement, the formation effect decreases faster than in normal media. The cement paste containing 10 wt.% silica produced 66% CSH in 8 hours and 25% more CSH in 24 hours, while CH decreased over 32% in 24 hours [8–14]. The chemical component of cement mainly comprises calcium silicate phases (i.e. C_3S and C_2S) and calcium aluminate phases (i.e. C_3A and C_4AF), and in the process of hydration of tricalcium and dicalcium silicate phases (C_3S and C_2S respectively) from calcium phases (C_3S and C_2S) calcium hydroxide (CSH) and calcium hydroxide (CH) are obtained [15].

According to several studies, there are three stages of the CSH process as the cause of the CSH formation when the additive is mixed with cement and composite materials. In the first phase, CSH presence is formed by a weak dissolution and a metastable permeation layer. The formation of etch pits has started at this stage, which is related to the level of regular and deep erosive alite. In the second phase, the transfer from separation acceleration increases, according to the second phase, the reason for the decrease and increase of the acceleration of CSH and forming needles in the SEM images of "ettringites" and relationship between additive materials and formation CSH is discussed. Third phase is related to the filling pore and voids. The most important index in the third phase is fill voids via additive in composite materials [16]. An example shows that the water-cement ratio can change the pore solution of hydrating C_3S in the first phase of CSH. According to this study, when the water-cement ratio increased from 0.4 to 0.75 metastable CSH and C/S and changed from 1.23 or 1.44 [17]. Moreover, several studies show that a reaction occurs when water comes into contact with cement hydrate in the first phase. In this way, hydrated layers are also formed, but hydrated layers are not visible to experimental tools and methods. It seems unlikely that the SEM results show that the crystallographic orientations exposed to CSH and C_3S are different [18-20]. The leading concept in the second phase is Nucleation and growth with impingement. According to Boundary Nucleation and Growth (BNG), hydrate hydrates form of cement grains' surfaces rather than uniformly in space. Avrami [21] described how the interaction between CSH hydrates from adjacent grains leads to a shift from acceleration to deceleration [22]. In general, according to the second phase of common minerals such as calcium carbonate, calcium sulfate, iron oxides, silica and alumina, the percentage has changed to follow the non-classical nucleation theory, so the nucleation theory is a valid theory considering some studies [15, 23, 24]. In addition, more evidence shows that the importance of the lack of water-filled pores is more important than the limiting critical size, the crystal growth and the depth of the void sizes that are directly related to the crystal growth. The results show that the small pores have a better effect on the formation of CSH crystals [25, 26].

Several studies were devoted to pozzolan additives to cement and concrete due to increase the CSH process and decrease the CH process. For example, Zhang et al. [27] found that when Carbon Nano Sheets (CNS), fly ash and SF were added to concrete, the micro cracks closed, CNS caused more CSH to be produced and affected the denser area of the Interfacial Transition Zone (ITZ). Gonzalez-Coneo et al. [28] investigated Raman and XRD analysis when SF was mixed with concrete. They found that the addition of SF to concrete can develop the CSH and hydration process faster than the normal situation. In addition, when SF is added to cement, the mechanical properties are increased and the water absorption is reduced. Al-kroom et al. [29] investigated on Dealuminated Kaolin (DK) as Alkali-Activated Slag (AAS) cement in a new method after activation called (FDK). They found that adding 10% FDK to concrete can fill the concrete microstructure with voids and also form CSH gel faster. In another example, Ijaz et al. [30] examined adding metakaolin (MK) and calcined clay (CC) to cement. They understood that when CC and MK added to cement, CSH process was significantly increased. Not only researchers added Micro Silica (MS) due to the formation of CSH, they added MS, because of improving strengths of concrete and reinforced concrete. For example, Chiadighikaobi et al. [31] reinforced High-Performance Concrete (HPC) by adding 3D printing trusses. In this way, HPC mixed with Silica to improved compressive and flexural strengths. In another example, Hematibahar et al. [32] compare results of reinforced concrete with 3D printing trusses and hyperboloid shell structures. In general, the additive materials application can not only format CSH but also improve the strength of concrete [33, 34].

Several studies investigated the indirect effects of the various additives on the cement matrix to form CSH. For example, the study by Shu & Zhang [35] demonstrated that incorporating 0.5% basalt fiber into concrete sped up the CSH process, as evidenced by SEM images showing distinct CSH crystals. In this case, basalt fibers could improve the

flexural strength and tensile strength because of the increase in the speed of CSH formation process [36]. Extensive research on the CSH process has been conducted within the cement and concrete industry [37-41]. Recent studies on the formation of calcium silicate hydrate by adding various additives (gypsum, calcium hydroxide, carbon nanofiber, fine recycled aggregate, and various nano-additives) and modeling the processes accompanying such formations have deeply addressed the microstructural changes of the studied materials, including SEM and EDS analyses. However, they primarily lacked a largely quantitative prediction of the elementary changes based on mixture proportions. In addition, there are few studies on the types of additives in cement and concrete [42, 43] and their influence on the CSH formation that should be detected by laboratory instruments.

The objective of this study is to investigate the effect of additives such as gelatin powder (GP), coffee grounds (SCG), peanut shells (PS) and silica fume (MS) in composite cementitious materials on the formation of calcium silicate hydrate (CSH) structure and to construct regression models of chemical elements such as calcium (Ca), silicon (Si), oxygen (O) and carbon (C) depending on the mixture composition. SEM and EDS are applied to study the composite cementitious materials. In fact, this study attempts to understand the cause of calcium silicate hydrate (CSH) by using SEM and EDS analyzes.

To fill the existing research gaps, this study goes beyond previous studies, which primarily focused on individual aspects of CSH formation without considering the convergence of structural and chemical analysis. Although many studies have examined the effects of additives on cementitious materials, they often lack a comprehensive examination of both CSH crystallization patterns (via SEM) and chemical composition modifications (via EDS). Furthermore, previous studies have largely ignored the quantitative prediction of elemental changes based on mixture proportions, limiting the ability to predict material behavior. By combining structural and chemical data, this study not only confirms the role of specific additives in accelerating CSH formation, but also identifies the phase-dependent effects of each material. This integrated approach provides a more complete, accurate, and practical basis for improving the mechanical and strength properties of cementitious composites, filling a critical research gap left by previous work.

The structure of the article is as follows. Section 2 describes all the materials and methods used in the study, Section 3 presents the results obtained in detail, Section 4 includes a final discussion of the results obtained, Section 5 contains conclusions on the results obtained in the study, Section 6 includes various declarations, and Section 7 provides references.

2. Material and Methods

Four different admixtures are used in the study: gelatine powder (GP), coffee grounds (SCG), peanut shells (PS) and silica fume (MS), moreover samples were cured under laboratory conditions without active control of temperature or humidity. The experimental process involves mixing these admixtures with the cement matrix and conducting SEM and EDS tests to observe the structural and chemical changes. For each mix design, SEM and EDS measurements were performed on three different regions of the sample to account for matrix heterogeneity, and the results were averaged. The Results section presents the SEM results confirming the crystallization of CSH and the EDS results showing the changes in the chemical composition. The discussion explains how the different admixtures affect the formation of CSH and its different stages and their role in changing the properties of cement. Using a regression approach, a predictive model is developed to accurately estimate changes in chemical composition using R^2 values. The regression model framework is adaptable to incorporate hydration time as a dynamic variable for modeling the evolution of CSH over extended curing periods.

The regression model presented in this study was developed based on the chemical composition and specific properties of the tested cement samples. Therefore, the high accuracy of the model is mainly guaranteed for ordinary Portland cements (OPC) and additives used in this study. However, by performing recalibration (i.e., adjusting the regression coefficients) based on experimental data for other types of cement, such as white cement or pozzolanic cements, the model can be made applicable to these systems as well. As a result, the model has the potential to be extended to other types of cement, but requires optimization and revalidation.

Figure 1 shows the process of predicting and modeling the formation of CSH in cementitious materials in a very step-by-step and systematic structure. It starts with defining the research objective and then selecting additives (such as gelatin, microsilica, coffee waste, and peanut shells). The next steps include preparing concrete samples, adding materials to the mixture, and curing the samples. Here, the flowchart is divided into two branches: structural analysis with scanning electron microscopy (SEM) to observe CSH crystals and chemical analysis with energy dispersive spectroscopy (EDS) to examine elemental changes. This clever division allows for a simultaneous analysis of the physical structure and chemical composition of the materials.

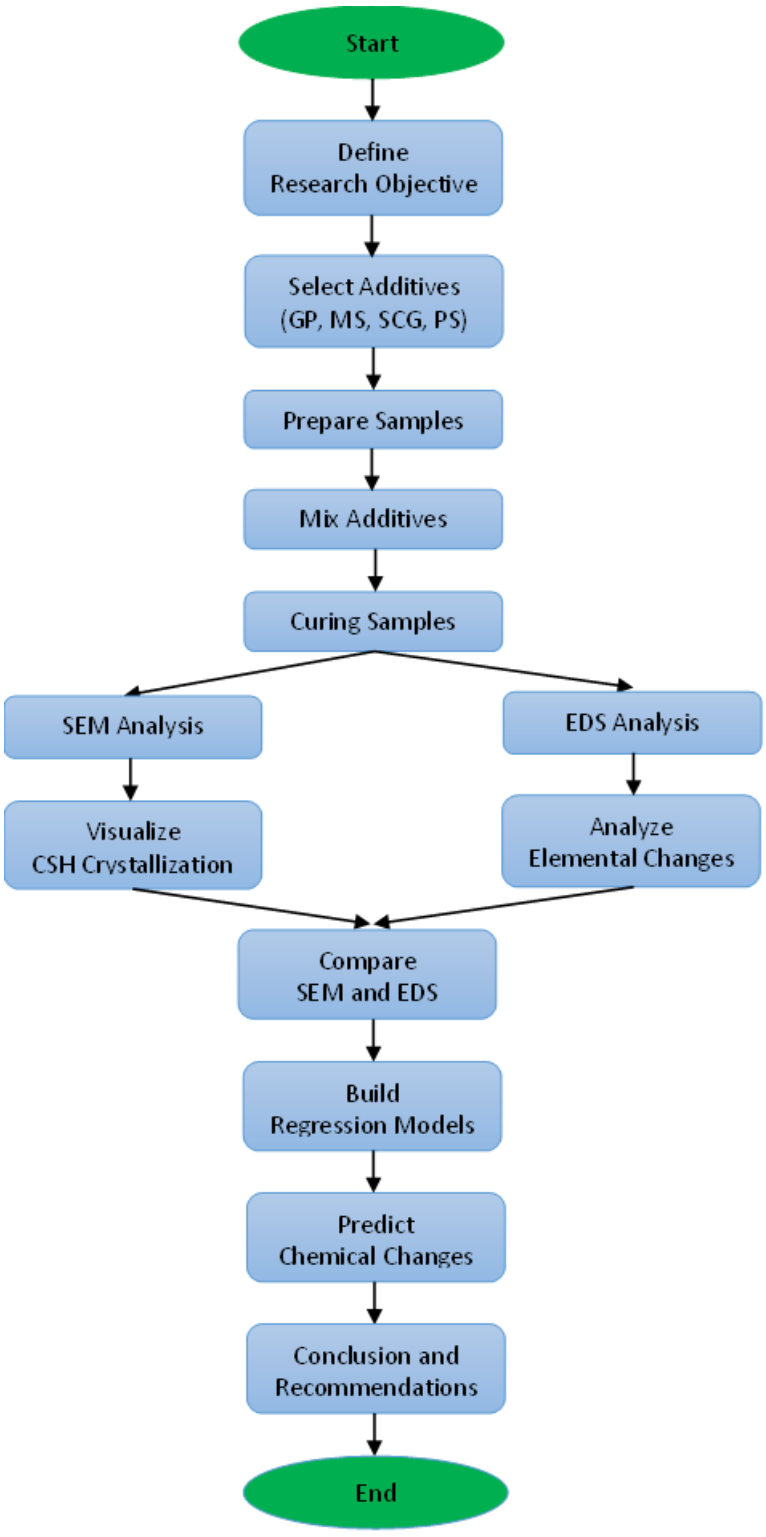

Figure 1. Flowchart of current study

Next, the SEM and EDS results are compared and regression models are built using them. These models are used to predict chemical changes and then their accuracy is evaluated with the R^2 index. The final steps include interpretation of results, integration of structural and chemical findings, development of optimal formulations, and presentation of final conclusions.

Figure 2 shows the process of preparing and performing experimental tests on concrete samples step by step and continuously. In the first stage, the concrete samples are displayed after loading or applying force, which represents the initial strength or load tests. These samples are then broken into smaller pieces to prepare them for more detailed analyses. Breaking the samples into smaller pieces allows for increased contact area and accuracy in subsequent tests, especially SEM and EDS tests.

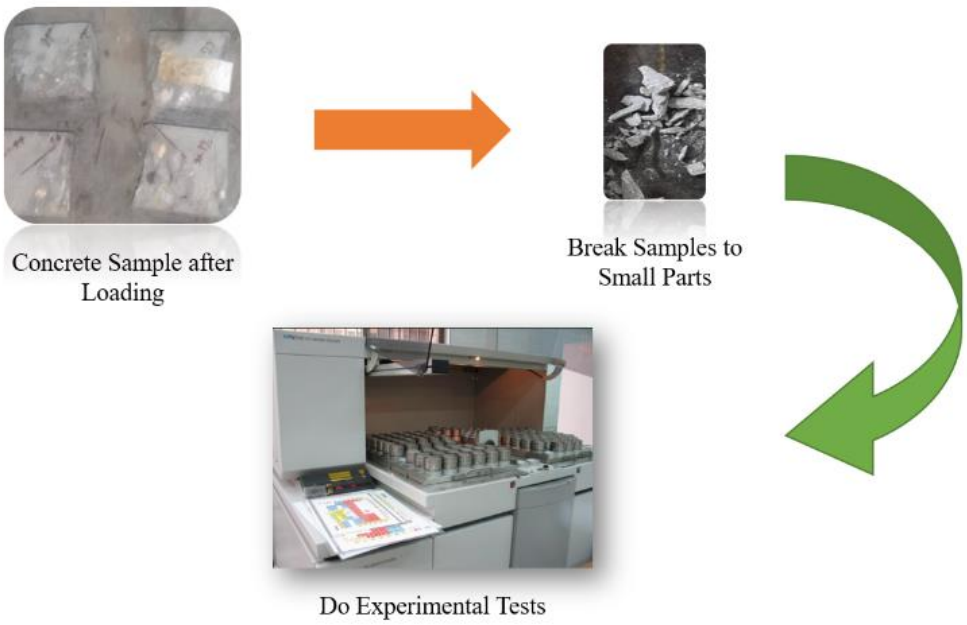

Figure 2. Experimental test operation

In the following process, the crushed samples enter the next stage for experimental tests, which is clearly shown in the image with specialized laboratory equipment.

2.1. Materials

To find the effect of various types of admixtures on CSH, gelatin powder (GP), coffee grounds (SCG), peanut shells (PS) and silica fume (MS) were used. Table 1 illustrates the mixture composition for each concrete sample.

CO-1 is the control sample when adding GP to concrete. According to Table 1, the control sample with cement is over 500 kg/m^3, fine aggregates are over 600 kg/m^3, coarse aggregates are over 450 kg/m^3 and super-plasticizer (SP) is over 10 kg/m^3. In addition, gelatin powder (GP) is added to the control sample. The chemical properties of cement are shown in Table 2. Table 3 illustrates the chemical composition of microsilica by X-ray fluorescence analysis (XRF) using Philips (Company) PW 2404 (Model).

Table 1. Various types of concrete mixtures

Samples	Cement kg/m^3	Water kg/m^3	Fine aggregates kg/m^3	Coarse Aggregates, kg/m^3	Marble Dust, kg/m^3	Super Plasticizer (SP), kg/m^3	GP, kg/m^3	SCG, kg/m^3	PS, kg/m^3	MS, kg/m^3
CO-1	500	190	600	450	-	10	-	-	-	-
GP	500	190	600	450		10	70	-	-	-
CO-2	550	176	-	-	1300	27.5	-	-	-	-
MS	450	148.5	-	-	1300	24.75	-	-	-	100
SCG	450	148.5	-	-	1300	29.25	-	40.5	-	100
PS	450	148.5	-	-	1300	31.5	-	40.5		100
CO-3	70	30	1000	-	-	-	-	-	-	-
M.C	70	30	1000	-	-	-	-	-	-	5

Table 2. XRF results of ordinary Portland cement (OPC) [38]

Oxide, %								Relative density
SiO_2	Fe_2O_3	MgO	SO_3	Al_2O_3	CaO	K_2O	L.O. I	
19.52	4.04	4.36	2.89	4.81	62.18	0.6	1.62	3.14

Table 3. XRF results of Micro Silica (MS)

Materials	Chemical Composite (%)
SiO_2	91.55
Al_2O_3	1.024
K_2O	1.73
MgO	1.02
Na_2O	0.52
Fe_2O_3	0.59
CaO	0.45
SO_3	0.35
P_2O_5	0.14
Cl	0.105
MnO	0.074
Zn	0.014
Pb	0.009
Rb	0.005
Sr	0.005
Cu	0.003
Ga	0.002
L.O. I	2.37

In other samples, CO-2 as another control sample 550 kg/m^3 cement, 176 kg/m^3 water, 1300 kg/m^3 marble dust and 27.5 kg/m^3, SP is cement material. In these types of samples, 100 kg/m^3 of MS was added to CO-2 (Figure 3), 40.5 kg/m^3 of SCG and PS were added to the cement material.

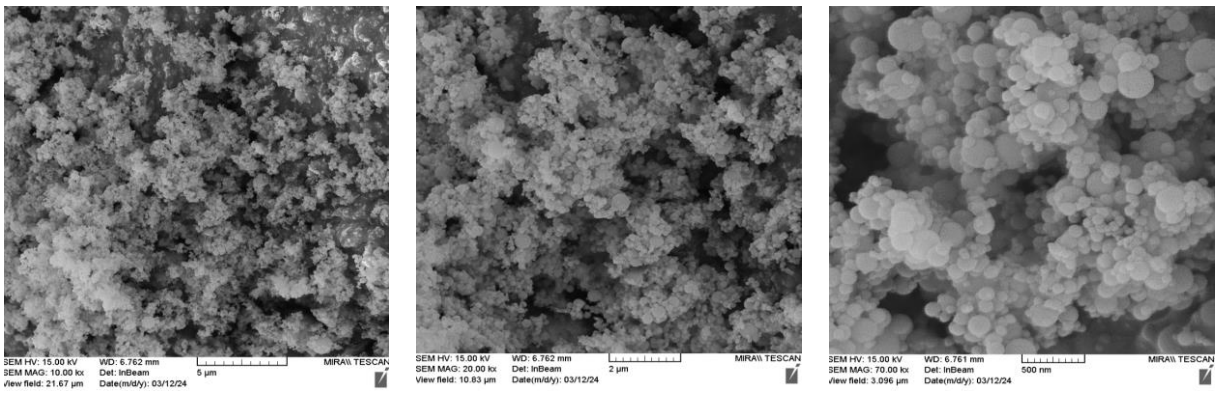

(a) (b) (c)

Figure 3. Micro silica FESEM results; (a) 5 µm, (b) 2 µm (c) 500 nm

The last type of concrete sample is Ultra-High-Performance Concrete (UHPC), with and without MS. UHPC-1 has more than 100 kg/m^3, while UHPC-2 is without MS.

2.2. Structural Analysis

The testing method in this paper is divided into two tests, SEM and EDS. According to the SEM experiments, the formation of crystals is the result of CSH, while the EDS results again show the chemical composition of each spot from SEM. Finally, these two ways can help us to improve the CSH process, which will be faster if we mix some additive with concrete or cement materials. The experimental device of SEM is TESCAN, produced by the Czech Republic. The device model is VEGA3. This model can also investigate the EDS experiments. In this model, the additional vacuum buffer significantly shortens the running time of the rotary vacuum pump.

2.3. Reliability of Prediction

In this study, R^2 is used to evaluate the effectiveness of the regression model in predicting the changes in chemical composition because of additives in cement materials.

$$R^2 = 1 - \frac{\sum_{i=1}^{n}(y_i - \hat{y}_i)^2}{\sum_{i=1}^{n}(y_i - \bar{y})^2}, \bar{y} = \frac{1}{n}\sum_{i=1}^{n} y_i \quad (1)$$

Here y_i is the actual observed value, $\hat{y}_i$ is the predicted value from the regression model, and $\bar{y}$ is the average of the observed values.

To determine the error of the proposed predictive approach, the formula was used;

$$Error = \frac{max|y_i - \hat{y}_i|_{sup}}{\hat{y}_i \, sup[y_1,\ldots,y_n]} \quad (2)$$

Thus, the error was determined in the upper range of y_i values.

3. Results

3.1. Composite Cementitious Materials Crystallization Results

Figures 4-a to 4-f shows that the crystal formation occurs rapidly when gelatin powder (GP) is added to concrete. Some studies prove that CSH crystals and needle crystals can be formed when GP is added to concrete [44]. Moreover, this acceleration of increase is related to the admixtures, which are related to the formation of CSH in concrete. According to Figures 4-d, 4-e and 4-f, the maximum crystal formation is shown, according to Scrivener et al. [16], crystallization occurred in the second phase of the three phases of CSH formation in cementitious materials, and the best CSH crystallization-related performance is observed at the water/cement ratio of 0.4 to 0.8 [45]. SEM analysis shows that the initial core of the CSH crystal formation process is close to crystals with sizes between 3 and 6 nm. Therefore, crystallization is also related to the nucleation and formation of CSH [46]. According to Figure 2-f, the maximum crystal size is less than 10 µm. A coarse and porous microstructure in the GP-modified cement matrix indicates that hydration reactions are still occurring. Dense crystalline structures resembling calcium silicate hydrate (CSH) formations are observed. A few acicular and cluster-like crystalline formations indicate the presence of secondary hydration phases, possibly ettringite or other hydration by-products. Small voids and cracks are present, which may be the result of shrinkage effects caused by the inclusion of gelatin powder. Needle formations indicate an increase in CSH and confirm that hydration processes are actively occurring. The presence of dense crystalline formations indicates an increase in the mechanical cohesion of the hydration products. Improved bonding with aggregates, a stronger interphase transition zone (ITZ) between the aggregates and the cement paste, shows an improvement in mechanical properties (Figures 4-a to 4-f).

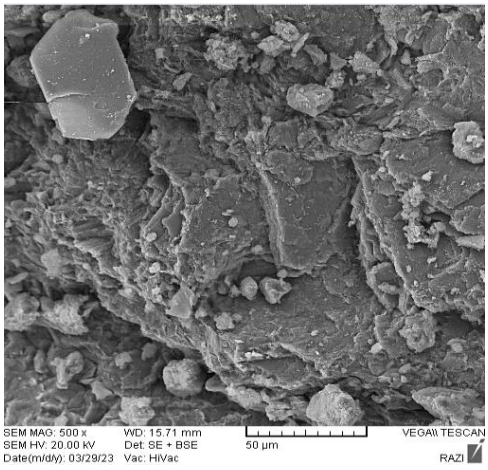

(a)

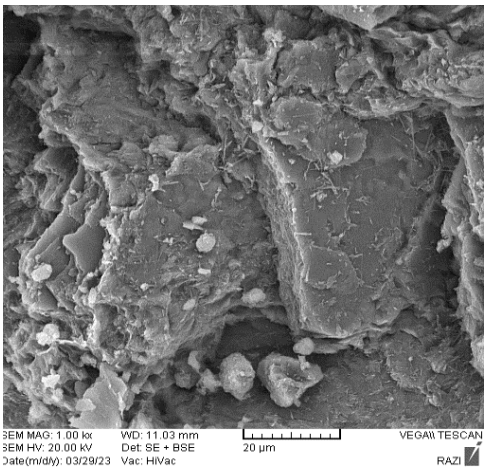

(b)

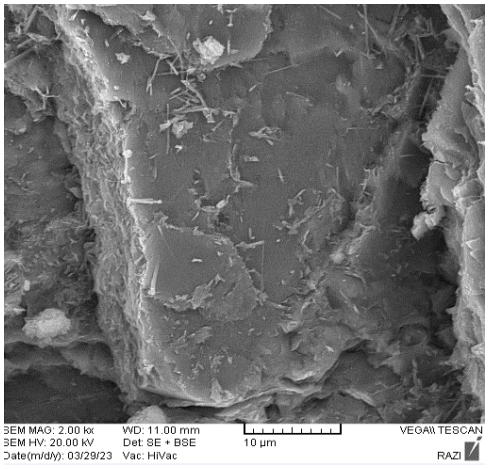

(c)

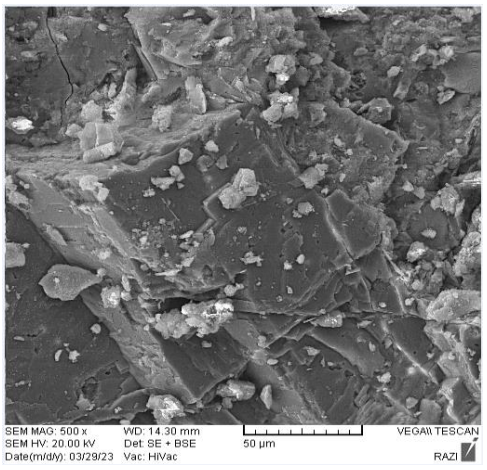

(d)

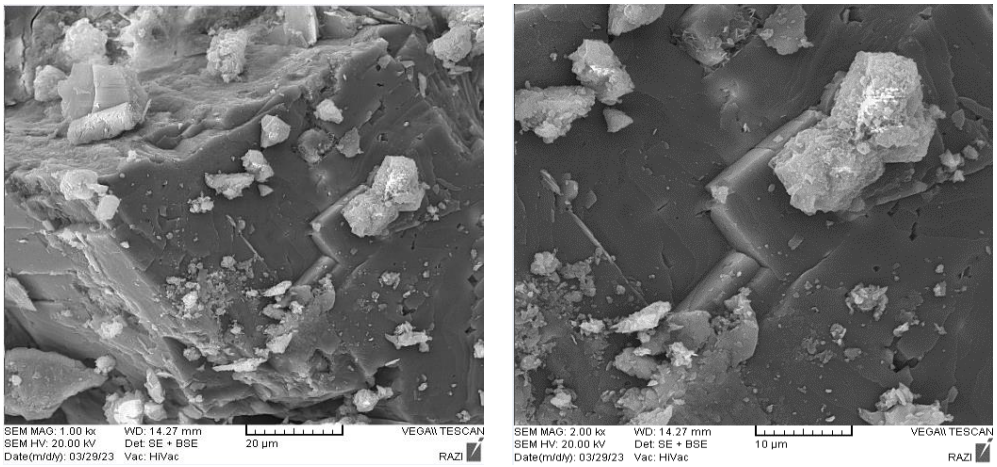

(e) (f)

Figure 4. Concrete with Gelatin Powder as additive; (a) CO-1 50 µm, (b) CO-1 20 µm, (c) CO-1 10 µm, (d) GP 50 µm, (e) GP 20 µm, (f) GP 10 µm

Visible cracks and micro voids indicate possible effects of early shrinkage or reduced water retention, which may be related to the organic nature of the gelatin powder. CSH formation is a key hydration product in cementitious materials, which significantly affects the development of strength and durability. The microstructure photographs in Figure 2 show the formation of colloidal gels, which are visible as amorphous clusters in SEM, and the initial nucleation of CSH crystals on the surface of the cement grains as well as the interaction of gelatin powder and hydration compounds. The growth of dense interconnected crystalline structures improves the strength of the material and strengthens the bonds between cement pastes and aggregates. A decrease in the number of voids because of continuous hydration is noticeable. The formation of denser CSH layers increasing the compressive strength and crystallization helps to improve the load-bearing capacity. Including gelatin powder (GP) in the cement matrix affects the microstructural characteristics due to the increased formation of CSH. SEM images confirm the denser growth of needle-like crystals, indicating rapid hydration.

In the CO-1 sample, a highly porous structure with larger pores due to slower hydration and incomplete gel formation and less C-S-H crystallization with fewer acicular formations was observed. A weaker bond between the cement pastes and aggregates was observed, resulting in more crack formation. A rough textured surface with unreacted cement grains was observed, indicating slower hydration reactions, while a dense, well-structured surface morphology with more C-S-H formations was characteristic of the modified GP sample. The structure showed smaller and more uniformly distributed pores, indicating higher hydration efficiency and more acicular structures of C-S-H, which enhanced crystallization. The gel-like hydration products visible in the matrix indicated better water retention (Table 4).

Table 4. SEM Comparison between CO-1 and GP

Feature	CO-1	GP
CSH Formation	Less dense, slower growth	Faster growth, more CSH crystals
Crystal Shape	Fewer needle-like formations	More structured CSH needles and gel
Pore Structure	Larger voids, more microcracks	Denser matrix, reduced porosity
Hydration Efficiency	Slower reaction, incomplete hydration	Accelerated hydration with more hydration products
Bonding Strength	Weak interfacial zones	Improved cohesion between paste and aggregates

Kaya [47] and Suksiripattanapong et al. [48] found that the addition of SCG to composite cementitious materials caused the accelerated formation of CSH crystals. According to their results, this process would occur in the first and second phase of the CSH formation process. In another example, when Ballesteros et al. [49] added SCG to composite cementitious materials, they found that CSH crystals increased rapidly.

When SCG and PS were added to the composite cementitious materials, the crystals with the size less than 10 µm were formed. The crystal size of CSH is related to the depth and size of the voids in the cement matrix. While the pores of the cement matrix are small, more specific crystals are formed, and while the pores of the cement matrix are larger, the formed crystals do not affect the mechanical properties [28] (Figure 5). The optimum growth size of CSH solution in the pores is about 10 nm, while the maximum size of CSH is less than 10 µm. This occurs when the voids are filled with water and partially saturated with cement. Therefore, the crystal structure is almost anisotropic [50, 51]. Figure 4 shows a similar situation. In Figure 4, when SCG and PS are added to the composite cementitious materials, the CSH

crystals have a similar situation. At low magnification (1300x), the overall surface appears uneven and heterogeneous, indicating a mixture of particles of different sizes. There are voids and micro cracks which may affect the mechanical strength and durability. Possible particles of anhydrated cement and embedded marble dust are visible, indicating an incomplete reaction in some areas.

At higher magnifications (1500x and 2500x), the hydrated products (CSH gel and $Ca(OH)_2$) are more obvious. Small acicular or fibrous structures may indicate the formation of ettringite, which is common in the early stage of hydration but may promote shrinkage cracking if present in excess. Marble dust particles appear to be embedded in the cement matrix and act as fillers. Some smooth areas indicate areas where the superplasticizer may be affecting the uniformity of hydration. SEM shows noticeable porosity, which affects the mechanical strength and permeability. Some interconnected pores indicate the risk of water penetration, which may affect the long-term strength. Cracks may be due to shrinkage due to hydration reactions. Insufficient adhesion is observed between the cement and marble dust. $CaCO_3$ (calcium carbonate) from marble dust appears in clusters, which probably reduces shrinkage, but also creates some unconnected areas. It acts as a filler, cleaning the pore structure, but excessive amounts can weaken the cement bond. The distribution of hydration products changes, which may be due to the dispersion of water by the super-plasticizer. This may explain some smoother areas in the microstructure, indicating better workability, but probably delays hydration in some areas.

The images show a dense and compact structure, indicating improved particle packing and a more refined matrix compared to CO-2. The presence of silica fume plays a critical role in reducing porosity and enhancing the formation of hydration products, particularly calcium silicate hydrate (CSH), which is responsible for the strength and durability of the material. At 1300x magnification, the surface appears significantly more cohesive, with fewer visible voids and cracks. The granular texture suggests that the hydration process is well advanced, resulting in the formation of tightly bonded particles. In contrast to CO-2, where unreacted cement particles and larger pores were observed, the MS sample exhibits a more continuous microstructure. This is likely due to the pozzolanic reaction of silica fume, which refines the pore structure by consuming calcium hydroxide and forming additional CSH gel. At 2500x magnification, the morphology reveals a more complex network of hydration products with fine, acicular and gel-like formations suggesting the presence of secondary CSH phases and possible ettringite formations. The fine particle distribution indicates improved dispersion of the silica fume, which increases the packing density and mechanical interlocking within the cement matrix.

The reduction in porosity at this scale suggests lower permeability, which is beneficial for long-term strength and resistance to aggressive environmental conditions. At 5000x magnification, the microstructure becomes even more detailed, revealing ultrafine hydration products with closely packed gel phases. Smooth areas visible in some regions indicate the influence of the superplasticizer, which improves workability by improving particle dispersion and reducing water requirements. Some nanoscale voids and small agglomerations of silica particles can be observed, but their minimal presence suggests a well-controlled reaction process. The overall microstructure at this magnification level confirms the increased density and homogeneity of the MS specimen compared to CO-2. The combination of cement, marble dust and silica fume results in a finer and less porous structure, which contributes to improved mechanical properties. The addition of silica fume effectively refines the hydration process by filling the voids and strengthening the overall matrix. Compared to CO-2, the presence of a denser network of CSH gel and pozzolanic reaction products suggests that the MS specimen will exhibit superior compressive strength, reduced permeability and increased durability. The interaction of the superplasticizer with the hydration products provides a homogeneous microstructure that minimizes weak zones and potential defects (Figures 5-d, 5-e and 5-f).

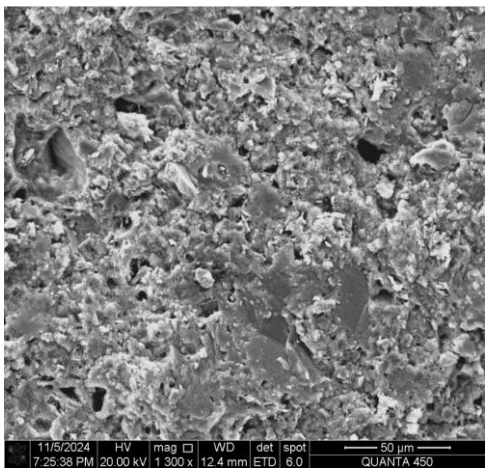

(a)

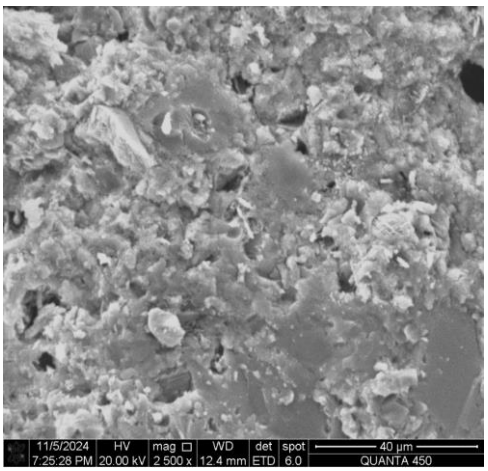

(b)

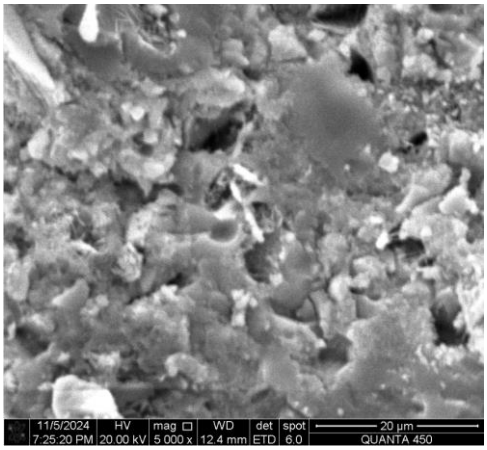
11/5/2024 7:25:20 PM
HV 20.00 kV
mag 5 000 x
WD 12.4 mm
det ETD
spot 6.0
20 µm
QUANTA 450

(c)

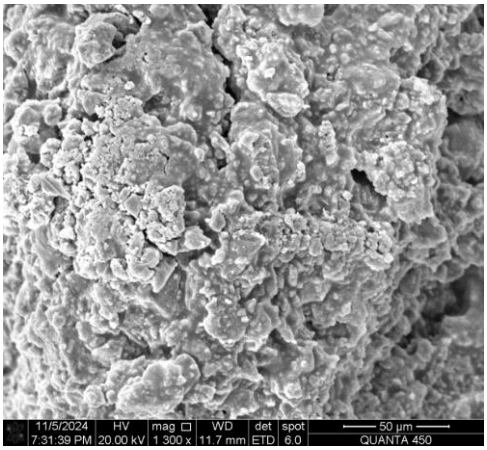
11/5/2024 7:31:39 PM
HV 20.00 kV
mag 1 300 x
WD 11.7 mm
det ETD
spot 6.0
50 µm
QUANTA 450

(d)

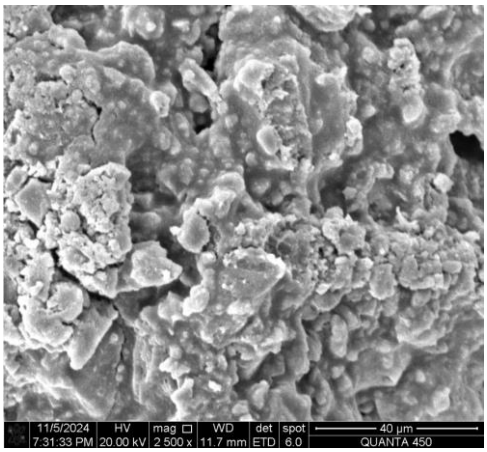
11/5/2024 7:31:33 PM
HV 20.00 kV
mag 2 500 x
WD 11.7 mm
det ETD
spot 6.0
40 µm
QUANTA 450

(e)

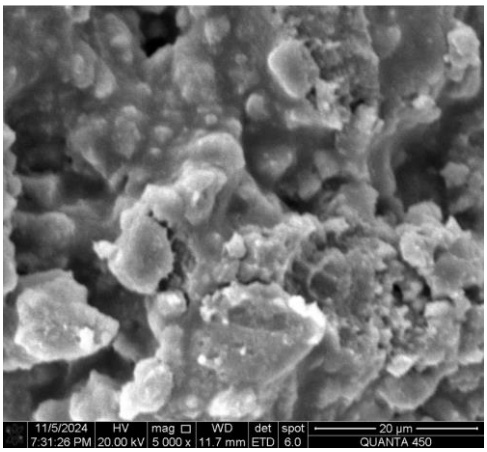
11/5/2024 7:31:26 PM
HV 20.00 kV
mag 5 000 x
WD 11.7 mm
det ETD
spot 6.0
20 µm
QUANTA 450

(f)

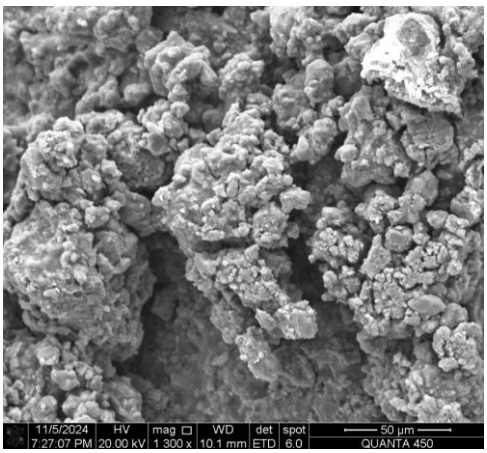
11/5/2024 7:27:07 PM
HV 20.00 kV
mag 1 300 x
WD 10.1 mm
det ETD
spot 6.0
50 µm
QUANTA 450

(g)

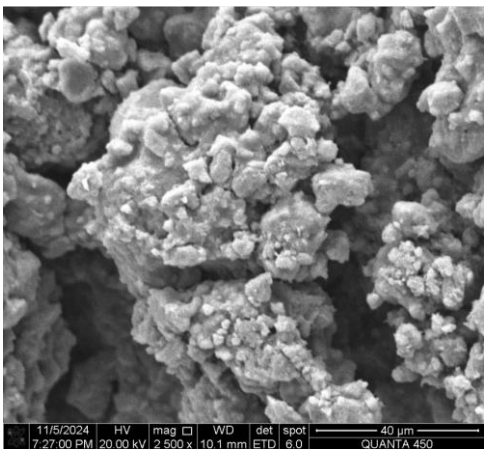
11/5/2024 7:27:00 PM
HV 20.00 kV
mag 2 500 x
WD 10.1 mm
det ETD
spot 6.0
40 µm
QUANTA 450

(h)

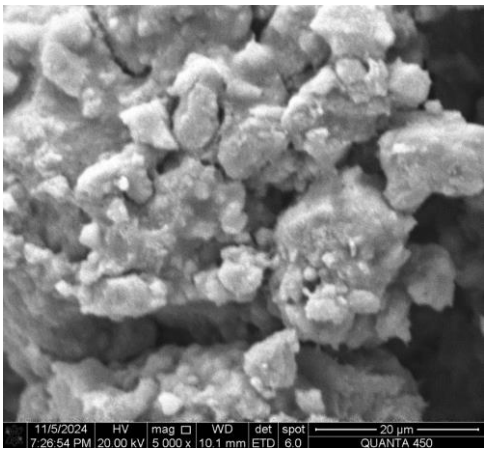
11/5/2024 7:26:54 PM
HV 20.00 kV
mag 5 000 x
WD 10.1 mm
det ETD
spot 6.0
20 µm
QUANTA 450

(i)

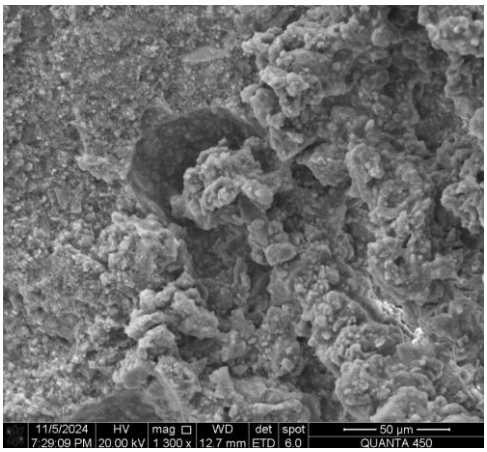
11/5/2024 7:29:09 PM
HV 20.00 kV
mag 1 300 x
WD 12.7 mm
det ETD
spot 6.0
50 µm
QUANTA 450

(j)

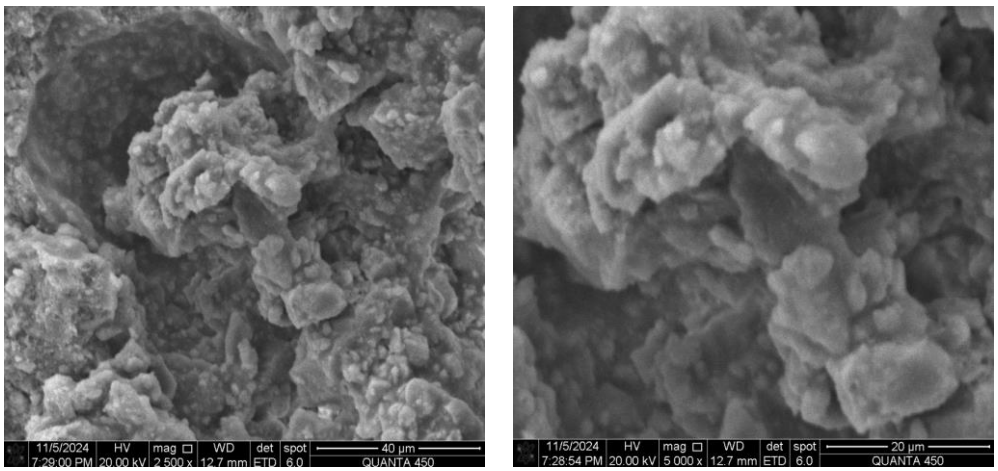

(k) (l)

Figure 5. CO-2, M.S, SCG and PS samples SEM; (a) CO-2 50 µm, (b) CO-2 40 µm, (c) CO-2 20 µm, (d) MS 50 µm, (e) MS 40 µm, (f) MS 20 µm, (g) SCG 50 µm, (h) SCG 40 µm, (i) SCG 20 µm, (j) PS 50 µm, (k) PS 40 µm, (l) PS 20 µm

Scanning electron microscope (SEM) analysis of the SCG sample, composed of cement, water, marble dust, superplasticizer (SP), coffee grounds (SCG) and silica fume, provides significant information on its microstructural characteristics. The surface morphology reveals a highly porous and loosely packed structure, distinguishing it from the CO-2 and MS samples. The presence of coffee grounds (SCG) appears to influence the microstructure, resulting in large surface roughness and particle agglomeration. In contrast to the more compact and well-formed microstructures observed in MS, the SCG sample exhibits a fragmented and coarse texture, which may affect both the mechanical performance and the durability. At 1300x magnification, the microstructure consists of large, rough clusters with visible gaps and weak bonding between the hydration products. The presence of SCG particles introduces organic matter into the cement matrix which may interfere with the hydration process, resulting in an increase in overall porosity. Compared to the denser MS sample, where the presence of microsilica improved the packing density, the SCG sample appears to have more voids and microcracks, suggesting reduced cohesion and weaker bonding between particles.

The hydration process appears to be less uniform, probably due to the influence of organic residues from the SCG which may have created localized areas of poor cement hydration. At 2500x magnification, the irregularity of the structure becomes even more apparent. The hydration products, including calcium silicate hydrate (CSH) and calcium hydroxide ($Ca(OH)_2$), appear dispersed, with loosely packed crystalline and gel-like formations. The pozzolanic reaction from the silica fume is visible in some areas, promoting additional CSH gel formation, but its effect does not seem to fully compensate for the degradation caused by the used coffee grounds. Compared to CO-2 and MS, where hydration was more developed, SCG shows a less well-defined distribution of hydration phases, promoting a more open and less compact structure. At 5000x magnification, the microstructure is dominated by small, loosely attached particles with less visible crystal growth compared to MS. The surface appears rough and fissured, indicating higher internal stress and greater potential for microcrack formation. The interaction of the superplasticizer (SP) with the hydration products appears inconsistent, as some areas exhibit smoother, well-hydrated surfaces, while others remain granular and underdeveloped. This variation suggests incomplete hydration due to the organic content of the SCG which may have absorbed water, limiting its availability for cement hydration. Additionally, some small voids and entrapped air pockets are visible, likely introduced by the spent coffee ground particles, which may have affected workability and compaction during specimen preparation. From this SEM analysis, it is evident that the SCG specimen has significantly higher porosity compared to the CO2 and MS, which is a result of the influence of the spent coffee grounds on the hydration kinetics and microstructure formation. The addition of microsilica does aid compaction in some areas, but the disruptive effect of the organic SCG particles results in an overall weakening of the higher permeability cement matrix.

Scanning electron microscope (SEM) analysis of PS sample, composed of peanut shell, cement, water, marble dust, superplasticizer (SP) and silica fume, provides critical insights into its microstructural characteristics and the influence of its organic component on hydration and matrix formation. The overall microstructure appears highly porous and irregular, indicating that the addition of peanut shell significantly disrupts the cement matrix, resulting in weaker particle bonding and increased voids. Compared with CO-2, MS and SCG samples, PS sample exhibits a more open and loosely compacted structure, which may affect both mechanical performance and durability. At 1300x magnification, the microstructure is fragmented, with visible voids and weak interparticle bonding. The organic nature of the peanut shell particles appears to have affected the hydration process by introducing gaps between the cement phases and reducing the overall cohesion of the matrix. The presence of large aggregates with visible cracks and air pockets suggests that water uptake by the peanut shell fibers may have affected the hydration kinetics, resulting in uneven phase development and a weaker cement bond.

In contrast to MS, where microsilica improved compaction, the PS sample appears to have a more disrupted matrix due to the interference of organic components. At 2500x magnification, the hydration products, primarily calcium silicate hydrate (CSH) and calcium hydroxide ($CaOH_2$), appear to be less uniformly distributed, with areas of poor cohesion and ruptures. The microstructure texture remains coarse and disordered, with poorly integrated hydration phases and weak interfacial bonding between the peanut shell fibers and the cement matrix. Microsilica particles do promote hydration enhancement in some areas, but the overall structure remains less dense compared to MS and SCG specimens. Superplasticizer (SP) can improve the initial workability, but its effect on hydration uniformity seems inconsistent due to the influence of the organic component. At 5000x magnification, specimen PS exhibits fine, loosely attached hydration products with numerous visible voids and porous structures. Unlike MS, where microsilica produced a well-packed microstructure, specimen PS exhibits poorly packed hydration products, resulting in a higher likelihood of microcracks and long-term structural weakness. The organic nature of the peanut shell particles appears to prevent complete bonding between the cement matrix and the hydration phases, creating weak zones that may adversely affect the mechanical properties. From this SEM analysis, it is evident that the addition of peanut shells significantly increases the porosity and disrupts the homogeneity of the hydration phases, resulting in a more open and weaker structure compared to the MS and SCG samples. While the silica fume promotes densification in localized areas, the organic nature of the polystyrene fibers creates weak interfacial zones that adversely affect the compressive strength and durability.

Sometimes the crystals are deformed into “needles” due to the curing conditions, in which case the needles grow on the surface around the peak heat release time [26]. Figure 5 shows that when MS was added to the composite cementitious materials, the needle state occurred. Some studies show that the acceleration period, curing periods and gradual nucleation are related to the growth and length of the needle. They realize that the growth of the deceleration period of CSH is related to the growth and length of the needle [52]. According to Figure 5-f, the maximum size of the needles is more than 2.5 μm, which shows that the size of the needles is related to the CSH crystals and their formation. Although Figure 6-c shows fewer needles than Figure 6-f, but when MS is added to sand cement, the volumes of the needles increase.

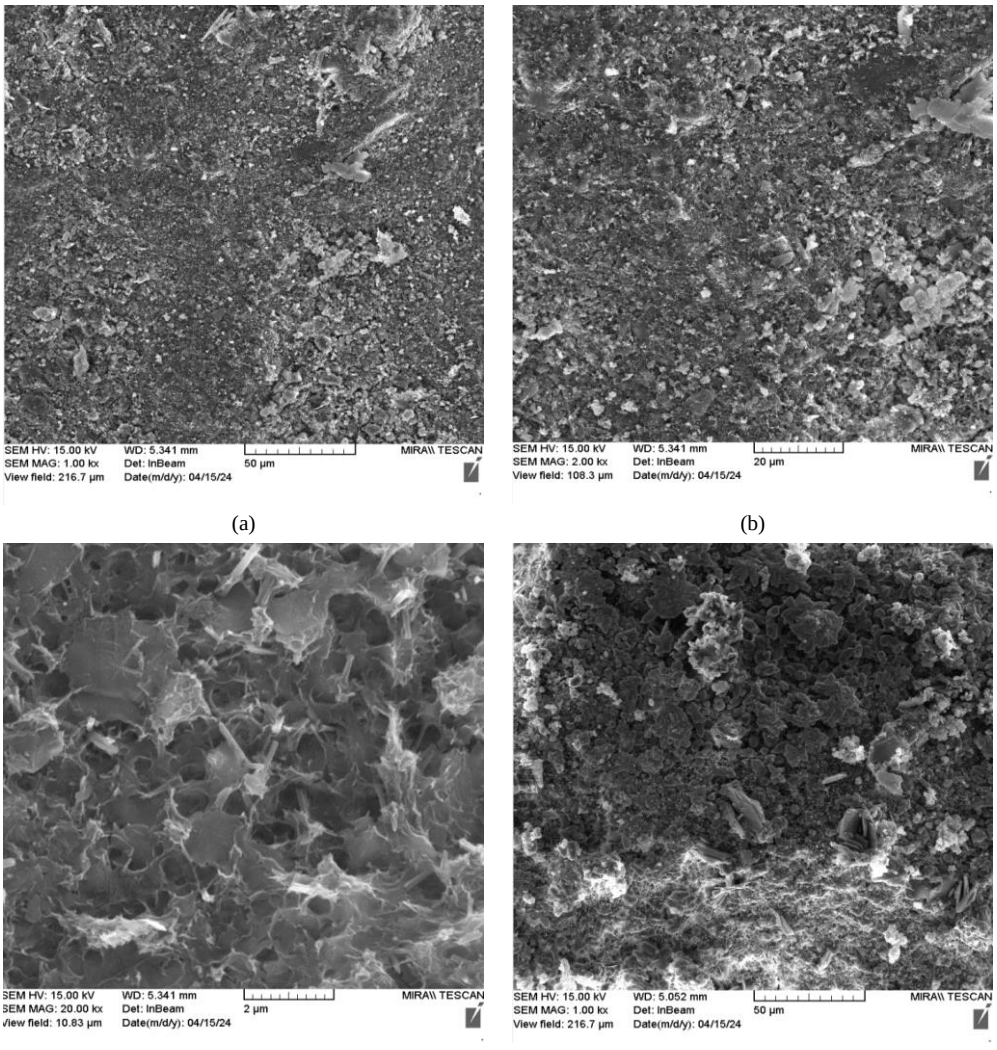

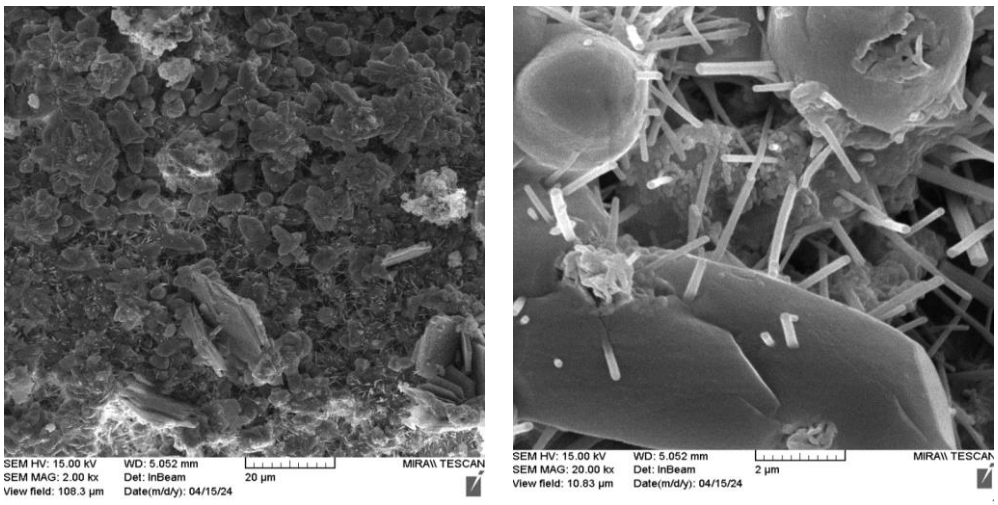

(e) (f)

Figure 6. Sand Cement with Micro Silica; (a) CO-3 50 µm, (b) CO-3 20 µm, (c) CO-3 2 µm, (d) MC 50 μm, (e) M.C 20 µm, (f) M.C 2 µm

Scanning electron microscope (SEM) analysis of CO-3 sample, which is composed of cement, water and cement sand (maximum 1000 kg/m³), provides significant information about its microstructural characteristics, hydration behavior and porosity. The microstructure has a more compact and homogeneous morphology compared to CO-2, MS and SCG, indicating better particle packing and hydration efficiency due to the presence of cement sand as a filler. At 1000x magnification, the surface appears relatively dense and continuous, with fewer visible voids and cracks compared to organically modified samples such as SCG and PS. The presence of well-integrated fine particles indicates a strong cement matrix, indicating efficient progress of the hydration process. Compared to the previous organically-added specimens, CO-3 exhibits a more cohesive structure, likely due to the fine-grained nature of the cement sand, which helps to reduce large air voids. At 2000x magnification, the surface texture reveals a fine network of hydration products including calcium silicate hydrate (CSH) and calcium hydroxide ($Ca(OH)_2$).

The CSH gel appears well distributed, forming a continuous binder phase that enhances strength development. The hydration phases are more compact, with less pronounced cracks and fewer interfacial gaps, suggesting that the cement sand helps to reduce internal stresses and shrinkage cracks. The uniform hydration of the cement particles further supports the improved mechanical stability of the specimen. At 5000x magnification, the microstructure shows well-developed hydrate gel formations, indicating advanced hydration reactions and strong bonding between the sand particles and the cement matrix. The porosity is significantly lower compared to SCG and PS, which had organic inclusions disrupting the microstructure. In CO-3, the cement sand particles appear embedded in the matrix, providing mechanical reinforcement and promoting compaction. Fine sand particles probably serve as nucleation sites for CSH formation, leading to a more compact structure. Several isolated voids and small microcracks are still visible, but their distribution was significantly reduced compared to the other samples, suggesting higher compressive strength and lower permeability. From this SEM analysis, it is evident that CO-3 has a well-compacted and purified microstructure with lower porosity and better integration of the hydration phase compared to samples containing organic materials such as SCG or PS.

Scanning electron microscope (SEM) analysis of MC sample, which is composed of cement, water, sand (maximum 1000 kg/m³), silica fume (5 kg/m³) and cement sand, provides a detailed evaluation of its microstructural characteristics, hydration and compaction behavior. The addition of silica fume plays an important role in increasing the compactness of the cement matrix, improving the particle distribution and reducing the porosity compared to other samples, such as CO-3 and SCG. At 1000x magnification, the surface appears to be closely packed with small hydration products distributed throughout the matrix, indicating efficient cement hydration and pozzolanic activity. The well-bonded structure suggests that silica fume has effectively filled the voids between cement particles, reducing the porosity and improving the durability. Compared to CO-3, which had a more granular and sandy texture, sample MC appears more refined, with fewer visible cracks and air voids. At 2000x magnification, the hydration products, primarily calcium silicate hydrate (CSH) and ettringite, form a tightly interwoven network that enhances mechanical strength and volumetric stability.

The CSH gel appears thinner and more uniformly distributed, supporting the hypothesis that sample MC has undergone an advanced hydration reaction due to the presence of microsilica. Acicular formations of ettringite are evident, suggesting an early stage of hydration that contributes to the initial development of strength and fracture toughness. The smaller particle size and increased surface area of the silica fume appear to have accelerated the pozzolanic reaction by consuming calcium hydroxide ($Ca(OH)_2$) and forming additional C-S-H which further

strengthens the matrix. At 20,000x magnification, the microstructure shows a highly refined and well-compacted hydration phase with distinct ettringite crystalline formations and a dense C-S-H gel network. The presence of fine silica fume particles in the matrix is evident, further confirming their role in enhancing the microstructure. In contrast to the coarse and porous textures observed in SCG and PS specimens, MC specimen exhibits a smooth, highly compacted and well-connected microstructure, indicating reduced permeability and increased compressive strength. The ettringite needle-like structures, along with the uniform distribution of CSH, suggest that the hydration process was efficient, resulting in the formation of a strong and durable cement matrix. From this SEM analysis, it is evident that MC has a highly compact and fine microstructure with superior hydration performance compared to CO-3 and SCG samples. The presence of microsilica significantly increased the compactness, reduced the porosity and improved the homogeneity of the hydration products.

3.2. Results of Chemical Composition of Composite Cement Materials

With the detection of CSH sign in concrete and the results of EDS, the first concrete with the addition of gelatin powder (GP) was investigated. GP can change the chemical properties inside the concrete due to the formatted crystals of CSH, this process is related to the second phase of the formation process of CSH [53]. Wang et al. [54] realized that in the formation process of CSH, $Ca(OH)_2$, $CaCO_3$, C_3S and C_2S are the causes of crystallized composite cement materials. It is obvious that when the formation of CSH is accelerated, the composite cement materials change. According to the results of Wang et al. [54], the chemical elements of calcium and oxygen increase. The results of EDS illustrate that when GP is mixed with concrete, the chemical elements of carbon, calcium and oxygen increase. Figure 7 shows the increase of the chemical elements of carbon, calcium and oxygen, and Table 5 shows the change of the chemical percentages of each element. Since, the formation of CSH is related to the curing time, the nanoscale of CSH is formed within 7 days, the maximum acceleration of CSH process occurs within 7 days of curing period, in addition, after 28 days of curing period, the acceleration of CSH is reduced, however, the maximum effect of increasing oxygen and calcium in EDS analysis is improved by $Ca(OH)_2$.

Therefore, the maximum increase of oxygen and calcium in concrete after adding GP to concrete occurs between 7 and 28 days of curing period [55]. With the addition of GP to concrete, the weight percentage of calcium increases from 1.48% to 31.39%, and the weight percentage of oxygen improves from 45.96% to 52.89%. Overall, the addition of GP to concrete increases the chemical elements related to the formation of CSH, and GP is effective in the formation of CSH. Ca and O are the dominant elements, confirming the active hydration reactions. The high presence of Ca suggests the accelerated crystallization of CSH, which leads to early strength development. The high oxygen content confirms the interaction of hydration water forming CSH and $Ca(OH)_2$. Silicon is the key element in the CSH gel and is critical for cement strength. The presence of 7.45% Si suggests good pozzolanic reactivity, potentially due to the interaction of microsilica or GP. SiO_2 increases the density of the matrix, reducing porosity and improving long-term strength. The increase in carbon (2.56%) confirms the effect of gelatin powder (GP). GP, an organic additive, affects the retention of hydration water and shrinkage. Higher presence of C can reduce early shrinkage but can also delay setting time. Potassium (K, 0.61%): probably from superplasticizers, improves cement dispersion. Magnesium (Mg, 2.50%): contributes to sulfate resistance, improves durability. Aluminium (Al, 1.48%): plays a role in ettringite formation, contributing to initial set and early strength. 12% Fe is present mainly as coarse aggregates or cement impurities with minimal effect on hydration, but may affect concrete color and durability. Interpretation of EDS data for cement hydration phases based on EDS composition (Figure 7, Table 5). When GP is added to concrete, the formation of CSH is accelerated due to the increase in calcium, oxygen and carbon.

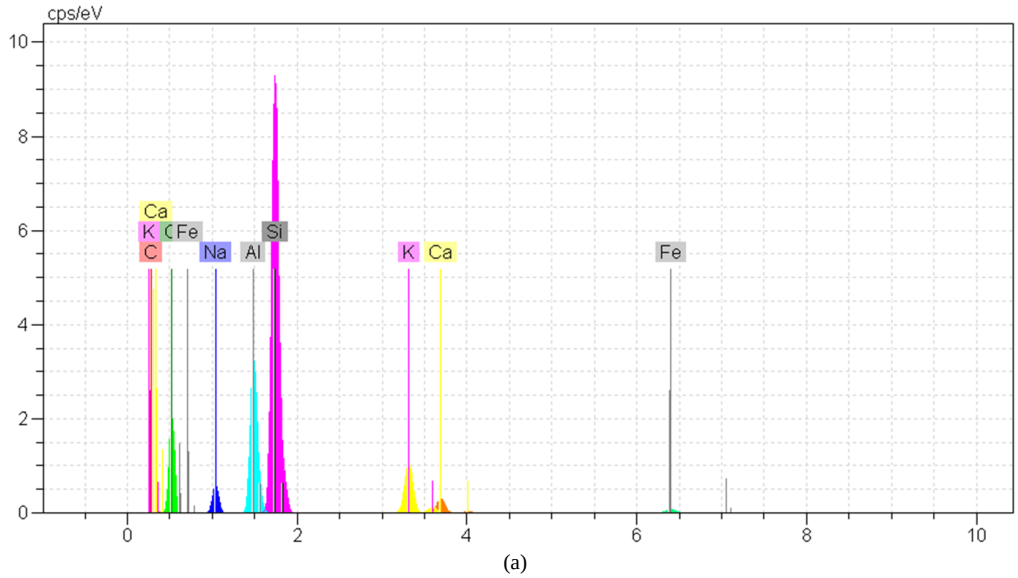

(a)

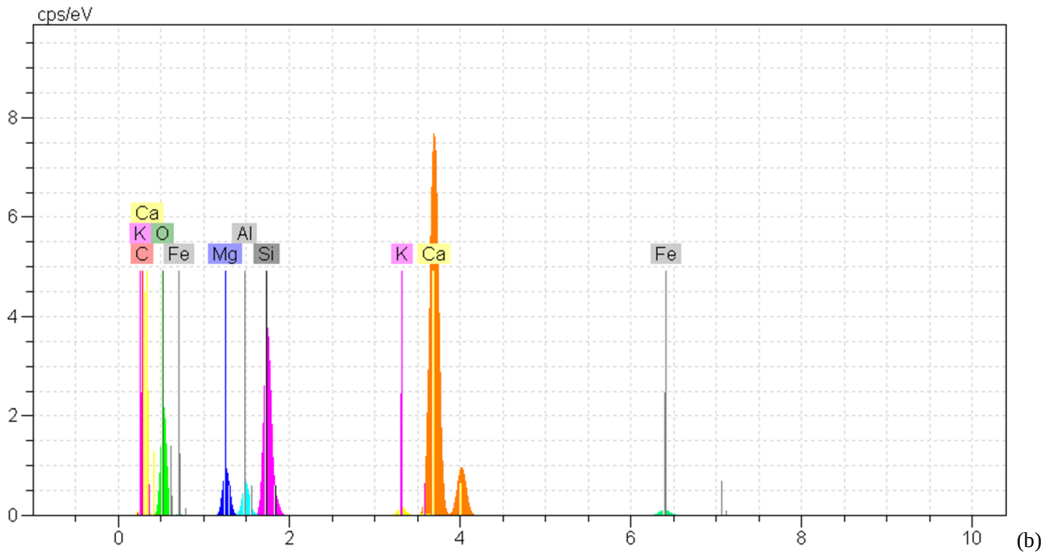

(b)

Figure 7. EDS results of concrete with additional Gelatin Powder (GP); (a) CO-1, (b) GP

Table 5. EDS results of concrete with additional GP

Sample/ Elements	Carbon	Oxygen	Sodium	Aluminum	Silicon	Potassium	Calcium	Iron	Magnesium
CO-1 (norm wt%)	1.11	45.96	2.99	11.01	31.43	5.10	1.48	0.93	-
GP (norm wt%)	2.56	52.89	-	1.48	7.45	0.61	31.39	1.12	2.50

With the addition of MS to the composite cementitious materials, the percentage of silica increased significantly from 1.79% to 6.12% according to Table 5, moreover, Figures 8-a and 8-b also confirm this increase. Berenguer et al. [56] added microsilica to concrete, they realized through EDS analysis that with the addition of microsilica to concrete, the percentage of silica increased significantly. Some studies show that 50% to 60% of the CSH formation phase in cement is due to the reaction of silicon, so the addition of microsilica and microsilica can accelerate the formation of CSH in composite cementitious materials [57]. Therefore, with the addition of microsilica to the control sample, the percentage of silica was improved (Table 5). According to Table 6 and Figure 8-c, the percentage of carbon and oxygen increased while the percentage of calcium and silicon decreased when SCG was added to the composite cementitious materials. Some studies show that SCG has more than 66.85% and 33.15% of the percentage of carbon and oxygen, respectively [58]. In fact, the increase in carbon and oxygen percentage in Table 6 due to the addition of SCG is due to the improvement of carbon and oxygen by the addition of SCG.

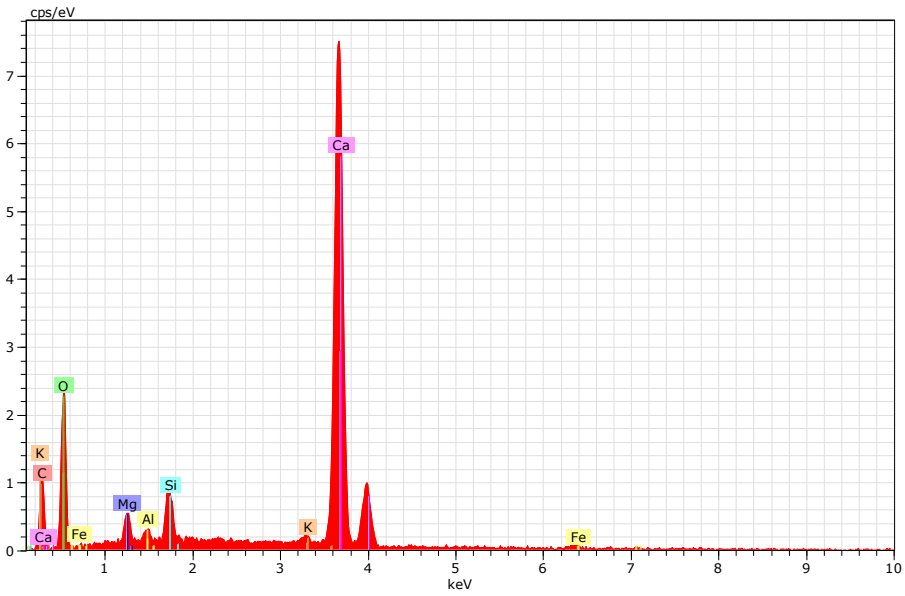

(a)

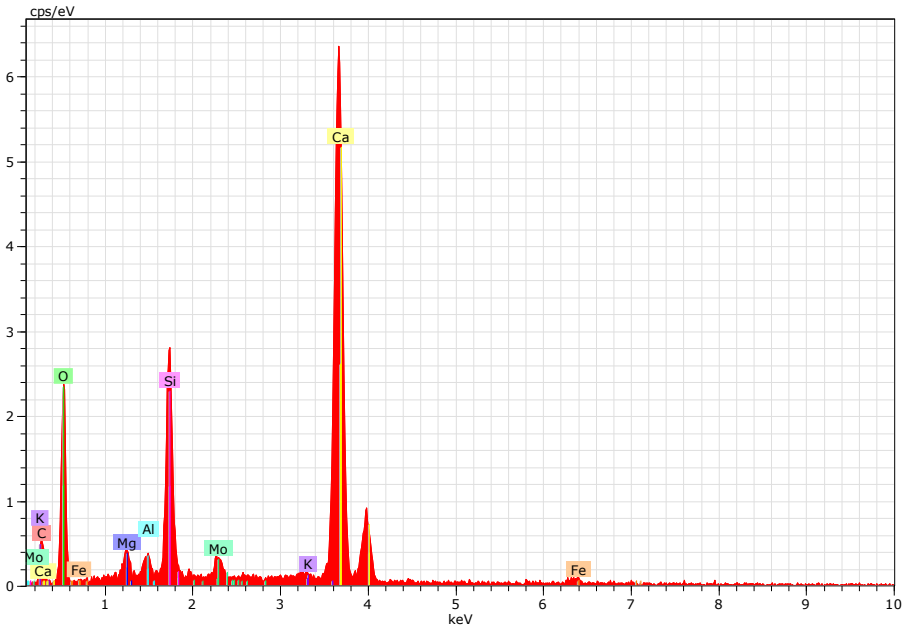

(b)

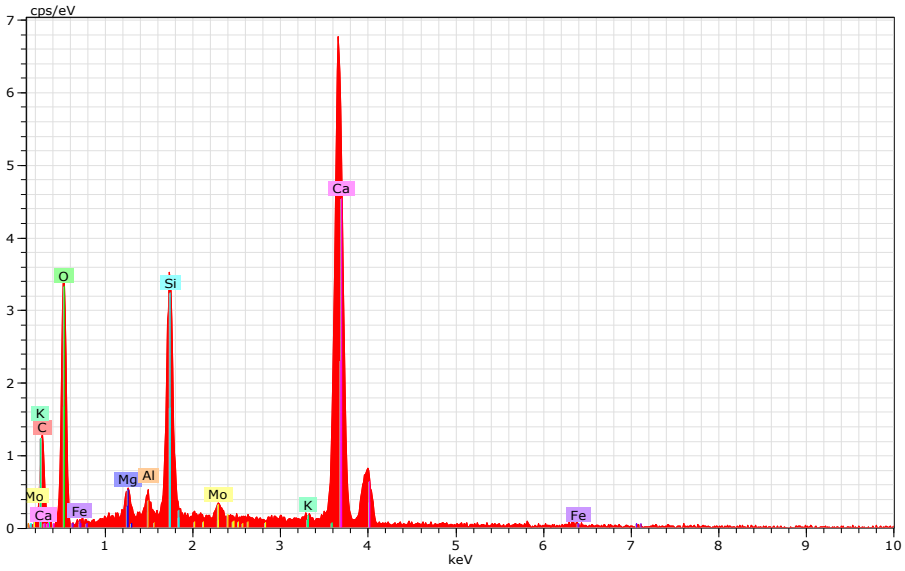

(c)

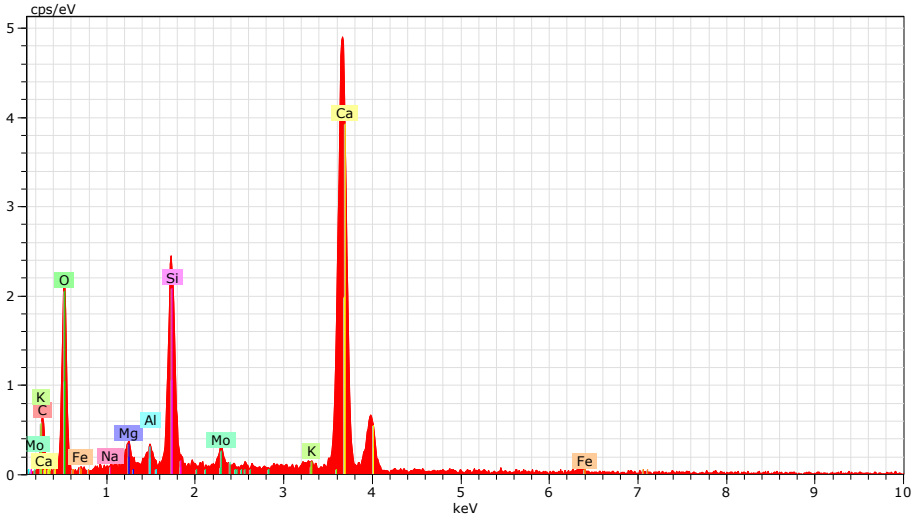

(d)

Figure 8. EDS results of: (a) CO-2, (b) M.S, (c) SCG, (d) PS

Table 6. EDS results of cement materials with additional Micro Silica, SCG and PS

Sample/ Elements	Carbon	Oxygen	Sodium	Aluminum	Silicon	Potassium	Calcium	Iron	Magnesium	Molybdenum
CO-2 (norm wt %)	10.80	48.92	-	0.39	1.79	0.64	17.35	0.66	1.41	-
M.S (norm wt %)	7.45	48.75	-	0.59	6.12	1.09	32.75	0.27	0.95	1.58
SCG (norm wt %)	13	51.60	-	0.40	5.05	0.91	27.40	0.20	0.70	0.74
PS (norm wt %)	9.33	49.74	0.07	0.61	6.53	1.04	29.76	0.54	0.96	1.42

Therefore, the role of SCG in the formation of CSH is in the third stage, and its greatest effect is to fill the voids [59]. The addition of PS instead of adding MS did not affect the percentage of silicon and calcium. According to Table 5 and Figure 8-d, when PS was added to the composite cementitious materials, the percentage of calcium and silicon did not change much instead of adding MS. However, PS did not affect the CSH formation process, biochar, a material derived from PS, can accelerate the formation of CSH in the first phase [60]. In fact, the produced active carbon from PS in biochar can accelerate the formation process of CSH [61].

Energy dispersive spectroscopy (EDS) analysis of the $CO2$ sample provides important information about its elemental composition, which directly affects its microstructural behavior and performance. The most dominant element detected is calcium (Ca), which is expected given the presence of cement and marble dust. The high intensity of the calcium peak confirms the significant presence of calcium-based compounds, mainly derived from calcium silicate hydrates (CSH), calcium hydroxide ($Ca(OH)_2$) and calcium carbonate ($CaCO_3$) from marble dust. This indicates that the hydration reaction has occurred to a significant extent, although the presence of unreacted particles suggests that a portion of the cement material remains unhydrated.

Oxygen (O) and carbon (C) are also present in significant quantities. Oxygen is essential for the hydration of the cement and is associated with the formation of C-S-H, which provides the mechanical strength of the material. Carbon, on the other hand, is probably derived from calcium carbonate in the marble dust, which acts as a filler. The presence of carbonates confirms that the marble dust is not completely dissolved in the cement matrix, which means that although it contributes to compaction, it can also act as an inert material in some regions. Silicon (Si) and aluminum (Al) are found in moderate quantities, indicating the existence of silicate phases, in particular C-S-H, which is responsible for the binding properties of the cement system. The presence of aluminum may be associated with aluminate phases, which can affect the early stage of hydration and setting time. The balance between these elements is critical, as silicates contribute to long-term strength development, while aluminates are often associated with early-stage reactions.

Magnesium (Mg), potassium (K) and iron (Fe) appear as minor elements. Magnesium may originate from cement impurities or additional materials, and its presence in small quantities does not significantly affect the mechanical properties. Potassium is commonly found in the clinker phases of cement and may influence alkali-silica reactions, although in this case, its low concentration suggests that it is not a serious problem. Iron, found in trace amounts, may be attributed to impurities or minor additions to the cement, contributing to coloration or minor hydration reactions.

From this EDS analysis, it can be concluded that the CO-2 sample is predominantly composed of calcium-rich phases, with secondary presence of silicates and aluminates supporting hydration processes. The significant amount of carbon suggests that the marble dust remains as a filler rather than an active participant in hydration. The presence of minor elements does not indicate any significant changes in the hydration of the cement, but may slightly affect the setting and durability properties. The interaction between the superplasticizer and the hydrated phases may have influenced the distribution of these elements, especially the formation of smooth areas observed in the SEM analysis (Figure 6-a). Energy dispersive spectroscopy (EDS) analysis of the MS sample consisting of cement, water, marble dust, super-plasticizer and microsilica provides a detailed insight into its elemental composition and the interactions between its components. The most dominant peak corresponds to calcium (Ca), indicating a strong presence of calcium-based compounds such as calcium silicate hydrate (CSH), calcium hydroxide ($Ca(OH)_2$) and calcium carbonate ($CaCO_3$) from both cement and marble dust. The intensity of the calcium peak suggests significant hydration and the presence of a well-developed cement phase, confirming the effective binding nature of the matrix.

Oxygen (O) is present in large quantities, as expected due to the formation of hydration products such as C-SH and ettringite, both of which contribute to the mechanical strength of the material. Carbon (C) is also detected, mainly originating from calcium carbonate ($CaCO_3$) in the marble dust, as well as potential organic residues of the superplasticizer. The presence of carbon further confirms that some amount of marble dust remains as a filler, influencing the microstructure by compacting the matrix, but does not actively participate in the hydration reactions. Silicon (Si) shows a significant peak, which distinguishes the MS sample from CO-2. This is explained by the presence of microsilica, which plays a decisive role in the pozzolanic reaction by consuming calcium hydroxide ($Ca(OH)_2$) and forming additional C-SH gel. The presence of higher silicon content suggests that the silica-rich phases have reacted efficiently, contributing to increased density, reduced porosity and improved mechanical properties. This confirms that the inclusion of microsilica results in a finer and more compact microstructure, as previously observed in the SEM analysis.

Aluminum (Al) is detected in moderate amounts, indicating the presence of aluminate phases that influence the early stages of hydration reactions and help control setting time. The formation of ettringite and other aluminate-based hydration products plays a role in the development of strength and long-term durability of the material. Magnesium (Mg) is also present, although in smaller amounts, probably due to cement impurities or minor additives. Its presence does not significantly affect the mechanical properties, but may slightly affect the hydration kinetics. Potassium (K) and iron (Fe) appear in trace amounts, probably due to cement clinker phases and mineral impurities. The presence of these elements suggests that the alkali-silica reaction potential is minimal, which is beneficial for long-term durability. Molybdenum (Mo), although present in small amounts, may be due to trace impurities or chemical additives included in the super-plasticizer formula. From this EDS analysis, it is evident that the MS sample exhibits a higher silicon to calcium ratio compared to CO-2, confirming the contribution of microsilica to the pozzolanic reaction. The reduction in free calcium hydroxide content, inferred from the high silica content, suggests a more advanced and refined hydration process, resulting in a denser and stronger microstructure. The presence of secondary hydration products, enhanced CSH formation and reduced porosity further support the hypothesis that the MS sample will exhibit superior mechanical properties, increased strength and lower permeability compared to CO-2 (Figure 8-b).

Energy dispersive spectroscopy (EDS) analysis of an SCG sample consisting of cement, water, marble dust, superplasticizer (SP), coffee grounds (SCG) and silica fume provides a detailed insight into its elemental composition and the interactions between its components. The dominant peak corresponds to calcium (Ca), confirming the strong presence of calcium-based compounds such as calcium silicate hydrate (CSH), calcium hydroxide ($Ca(OH)_2$) and calcium carbonate ($CaCO_3$) from cement and marble dust. The intensity of the calcium peak suggests that the cement phase remains the main binder, but the irregular hydration patterns observed in the SEM images indicate that the overall hydration process might have been disturbed by the presence of SCG particles. Oxygen (O) is present in significant quantities, mainly related to the hydration process and the formation of CSH gel and ettringite. The relatively high oxygen content suggests ongoing hydration, but SEM analysis showed less uniform hydration products, implying that the distribution of water in the cement matrix may not have been optimal.

Carbon (C) also appears in high quantities, significantly higher than in CO-2 and MS, which is a direct result of the addition of spent coffee grounds (SCG). The organic nature of the SCG contributes additional carbon to the mixture, confirming that some organic residues remain even after hydration. This increased carbon content correlates with the higher porosity observed in the SEM, as the organic particles may have interfered with hydration, leading to the formation of localized voids and weak zones in the matrix. Silicon (Si) appears in significant amounts, mainly attributed to the silica fume and silicate phases in the cement. The presence of silica fume promotes pozzolanic reactions by consuming calcium hydroxide ($Ca(OH)_2$) and forming additional C-S-H gel, which is expected to increase strength and reduce porosity. However, the irregular hydration patterns observed in SEM indicate that the pozzolanic effect may not have completely neutralized the negative impact of SCG on the hydration process. Compared to MS, where silica fume effectively compacted the matrix, the SCG sample shows a more dispersed silica phase, suggesting that the interaction of silica fume with cement may have been less effective due to interference from the SCG particles.

Aluminium (Al) is found in moderate concentrations, indicating the presence of aluminate phases such as ettringite, which play a role in the early setting reactions. The distribution of aluminium suggests some level of phase separation, possibly related to the uneven hydration process observed in the SEM. Magnesium (Mg) is present in smaller amounts, probably due to cement impurities or trace additives. The low Mg content suggests that it does not significantly influence the hydration process. Potassium (K) and iron (Fe) appear in trace amounts, mainly from cement clinker phases and natural impurities. Potassium, as an alkaline component, can influence alkali-silica reactions (ASR), but its low concentration suggests a minimal effect in this case. Molybdenum (Mo) is found in minor amounts, possibly introduced through chemical impurities or SCG residues. From this EDS analysis, it is evident that the SCG sample has a significantly higher carbon content, confirming the organic influence of the used coffee grounds on the hydration process. While calcium and silica remain dominant, suggesting continued CSH formation, disturbances caused by the organic matter appear to interfere with the normal hydration sequence. The higher oxygen content confirms the presence of hydration phases, but their uneven distribution, as seen in the SEM, suggests a less compact and more porous microstructure. Energy dispersive spectroscopy (EDS) analysis of the PS sample, consisting of peanut shells, cement, water, marble dust, super-plasticizer (SP) and silica fume, provides detailed insight into its elemental composition and hydration behavior. The dominant peak corresponds to calcium (Ca), confirming the strong presence of calcium-based compounds such as calcium silicate hydrate (CSH), calcium hydroxide ($Ca(OH)_2$) and calcium carbonate ($CaCO_3$), mainly derived from cement and marble dust. The high calcium intensity suggests that the cement phase remains the main binder, but the porous microstructure observed in SEM suggests that the hydration process was influenced by the presence of peanut shell particles.

Table 6 illustrates that when MS was added to the composite cementitious materials (sand cement) only the percentage of silica increased from 21.73% to 26.77%. Therefore, the water to cement ratio in this mixture was lower than other mixtures, it is important to analyze the effect of water on the formation process of CSH. MS with high potential of SiO_2 is able to interact with water molecules very effectively through hydrogen bonding, thus the interaction

of MS with water molecules in cementitious materials is related to the capacitive aspect of the nature of cement [62]. According to Table 6 and Figure 9, MS plays a role of filler after accelerating the CSH process. Some studies prove that the increase in the surface contact of cement and MS with water is one of the important aspects as a filler effect and is responsible for the high dispersion of cement grains in the fresh state. Therefore, the role of MS in this sample is more than the role of filler to accelerate CSH [63, 64].

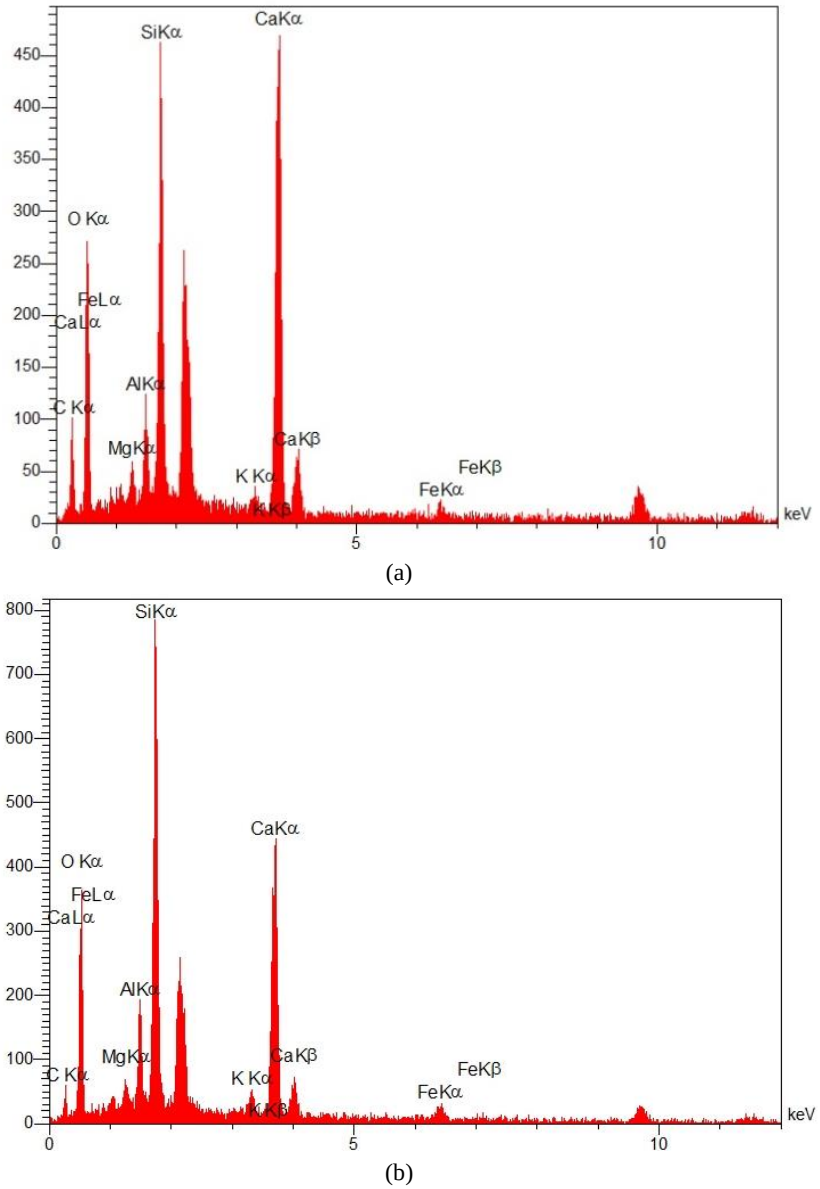

Figure 9. EDS results of: (a) CO-3, (b) M.C

Energy dispersive spectroscopy (EDS) analysis of a CO-3 sample consisting of cement, water and cement sand (maximum 1000 kg/m³) provides a detailed insight into its elemental composition, hydration behaviour and material properties. The most dominant peak in the spectrum corresponds to calcium (Ca), confirming the presence of calcium-based compounds such as calcium silicate hydrate (CSH), calcium hydroxide ($Ca(OH)_2$) and calcium carbonate ($CaCO_3$), all of which contribute to the bonding and strength development of the cement matrix. The high calcium intensity suggests a well hydrated structure in which the cement reactions have taken place efficiently. Oxygen (O) is detected in high quantities, indicating the formation of hydration products such as CSH and ettringite, which play a decisive role in the mechanical strength and durability. The strong presence of oxygen suggests a well-developed hydration phase, confirming the observations made in the SEM analysis where a dense and compact matrix was visible. The presence of carbon (C) is relatively low compared to SCG and PS samples, indicating the absence of significant organic interference in this sample, which facilitates better hydration and reduced porosity. Silicon (Si) appears in significant amount, derived from both cement and cement sand. The presence of silicon-rich phases supports pozzolanic reactions where silica reacts with calcium hydroxide to form additional C-S-H gel, resulting in increased strength and durability. Compared to SCG and PS samples, in which hydration was impaired due to organic components, sample CO-3 exhibits a higher Si/Ca ratio, indicating a more developed cement phase with improved structural integrity.

Aluminium (Al) is present in moderate quantities, confirming the presence of aluminate phases such as calcium aluminate hydrates (CAH) and ettringite, which contribute to setting time control and early strength development. The distribution of aluminium is relatively uniform, suggesting that cement hydration has occurred efficiently without phase separation. Magnesium (Mg) is found in smaller quantities, probably originating from cement clinker phases or impurities in the cement sand, but its influence on the hydration behavior remains minor. Potassium (K) and iron (Fe) are present in trace quantities, mainly from cement clinker phases and mineral impurities. The low concentration of potassium suggests a minimal risk of alkali-silica reactions (ASR), which is beneficial for long-term strength. The presence of iron (Fe) is also minor, indicating that it does not significantly influence hydration, but may contribute to color changes or minor phase modifications. Molybdenum (Mo) is found in trace amounts, possibly introduced via trace mineral impurities. From this EDS analysis, it is evident that the CO-3 exhibits a well-balanced elemental composition with a strong calcium silicate presence contributing to a well-hydrated and structurally stable cement matrix (Figure 9-a).

Energy dispersive spectroscopy (EDS) analysis of MC sample consisting of cement, water, sand (maximum 1000 kg/m³), silica fume (5 kg/m³) and cement sand provides essential information on the elemental composition, hydration behaviour and performance characteristics of the material. The dominant peaks correspond to silicon (Si) and calcium (Ca), indicating a high presence of calcium silicate hydrate (CSH), calcium hydroxide ($Ca(OH)_2$) and silicate-based compounds, which are crucial for the development of strength and durability. Compared with CO-3, the higher silica intensity in MC suggests an enhanced pozzolanic activity, probably due to the inclusion of silica fume. The Si/Ca ratio in MC is markedly higher than in CO-3, which generally correlates with a denser microstructure, improved mechanical properties and reduced porosity.

Oxygen (O) appears in high amounts, confirming the formation of hydration products such as CSH and ettringite, which contribute to mechanical strength and durability. The strong presence of oxygen suggests a well-developed hydration phase, consistent with SEM analysis, where a highly compact structure with purified hydration products was observed. The relatively low carbon (C) content compared to organically modified samples such as SCG and PS confirms that no significant organic interference is present, which is beneficial for hydration homogeneity and reduced void formation.

Silicon (Si) is a major element, mainly contributed by microsilica and silicate phases in cement. The higher silica content compared to CO-3 indicates a stronger pozzolanic reaction, where silica reacts with calcium hydroxide to form additional CSH, resulting in increased strength and durability the fine dispersion of silica in the cement matrix results in better particle packing and reduced permeability, as seen in the SEM images. Aluminium (Al) is found in moderate amounts, indicating the presence of aluminate-based phases such as calcium aluminate hydrates (CAH) and ettringite, which affect the early stage of hydration, setting time and long-term durability. The uniform distribution of aluminium suggests that the hydration process was uniform, enhancing structural stability. Magnesium (Mg) is found in smaller amounts, probably derived from cement clinker phases or minor impurities. Although its effect on hydration is relatively minor, it can contribute to minor phase changes and additional hydration products. Potassium (K) and iron (Fe) are present in trace amounts, mainly from cement clinker and mineral admixtures (Table 7). The low concentration of potassium implies a minimal risk of alkali-silica reaction (ASR), which is beneficial for long-term strength. The presence of iron (Fe) is also minor and does not significantly affect hydration, but can contribute to discoloration or minor changes in the stability of the microstructure. From this EDS analysis, MC exhibits a high silicon content compared to calcium, confirming the increased pozzolanic activity and the role of silica fume in improving the cement matrix (Figure 7-b).

Table 7. EDS results of cement materials with additional Micro Silica, SCG and PS

Sample/ Elements	Carbon	Oxygen	Aluminium	Silicon	Potassium	Calcium	Iron	Magnesium
CO-3 (norm wt%)	9.03	27.19	4.83	21.73	0.45	19.25	1.18	1.72
M.C (norm wt%)	5	25.36	7.02	26.77	1.05	15.33	1.75	2.03

When MS, SCG and PS were added to composite cementitious materials, microsilica caused the development of silicon and played a major role in accelerating the formation of CSH. When adding SCG to composite cement materials, the percentage of oxygen and carbon increased. Although this situation is the reason for the acceleration of CSH formation, but this process is likely to fill the voids in the third phase of CSH formation process. Moreover, mixing PS has no positive effect on the acceleration of CSH according to the EDS results. In general, microsilica formed CSH process in the first and second phases. SCG plays the role of a filler in the formation of CSH and accelerates the CSH process by increasing the chemical elements of carbon and oxygen.

3.3. Predicting Chemical Elemental Composition Using EDS and Mix Materials

To create a general prediction equation for the EDS elemental composition based on concrete mix materials, we need a generalized model that includes the mix proportions and EDS weight percentages of key elements such as calcium (Ca), silicon (Si), oxygen (O), and carbon (C).

In this situation, Equation 3 is:

$$C_x = f + aW_C + bW_{FA} + cW_{CA} + dW_{SP} + eW_A \quad (3)$$

here, C_X is the predicted weight percent of chemical element *X* (e.g. Ca, Si, O, C) from EDS analysis, W_C is the cement content (kg/m³), W_{FA} is the fine aggregate content (kg/m³), W_{CA} is the coarse aggregate content (kg/m³), W_{SP} is the super-plasticizer content (kg/m³) and W_A is the additive content (e.g. Gelatin Powder (GP), Micro Silica (MS), Coffee Grounds (SCG), Peanut Shells (PS)), *a*, *b*, *c*, *d*, *e* and *f* are the regression coefficients.

The regression models (4) – (7) developed to predict the weight percent of calcium (Ca), silicon (Si), oxygen (O) and carbon (C) in cementitious materials were estimated using the R^2 index on a sample of 1000 values for each parameter.

$$C_C = 6.80 + 0.0008W_C - 0.00473W_{FA} - 0.00721W_{CA} + 0.00622W_{SP} + 0.0923W_A, R^2 = 0.924 \quad (4)$$

$$C_{Ca} = 17.58 + 0.00164W_C - 0.01732W_{FA} - 0.02558W_{CA} + 0.5157W_{SP} - 0.1318W_A, R^2 = 0.988 \quad (5)$$

$$C_{Si} = 18.05 - 0.00177W_C + 0.01409W_{FA} + 0.02124W_{CA} - 0.3960W_{SP} + 0.0140W_A, R^2 = 0.985 \quad (6)$$

$$C_O = 45.58 + 0.00044W_C - 0.00044W_{FA} - 0.00122W_{CA} + 0.1061W_{SP} + 0.0405W_A, R^2 = 0.910 \quad (7)$$

The R^2 value measures how well the independent variables (cement, fine aggregate, coarse aggregate and admixtures) explain the variance in EDS weight percent. A value close to 1 indicates a stronger correlation between the model predictions and the actual experimental data. The results show that calcium (Ca) has the highest R^2 value of 0.988, followed by silicon (Si) with 0.985, indicating that the regression model does a good job of predicting these elements. Carbon (C) has an R^2 value of 0.924, which is still acceptable but shows some bias. Oxygen (O) has the lowest R^2 of 0.910, indicating that the model has difficulty accurately predicting oxygen content, possibly because of variations in hydration reactions and uncontrolled environmental factors affecting oxygen levels in the cement matrix.

From a practical perspective, the model provides a useful assessment tool for predicting EDS composition in cementitious materials, especially for calcium and carbon, which are critical for assessing cement hydration and strength development. However, refinements such as inclusion of water to cement ratio, curing time, and additional chemical reactions affecting oxygen and silicon content can improve the accuracy of prediction. The reliability of prediction in the form of the coefficient of determination R^2 (Figure 10) and the maximum deviation measured in the upper range of Error values, % are presented in Table 8.

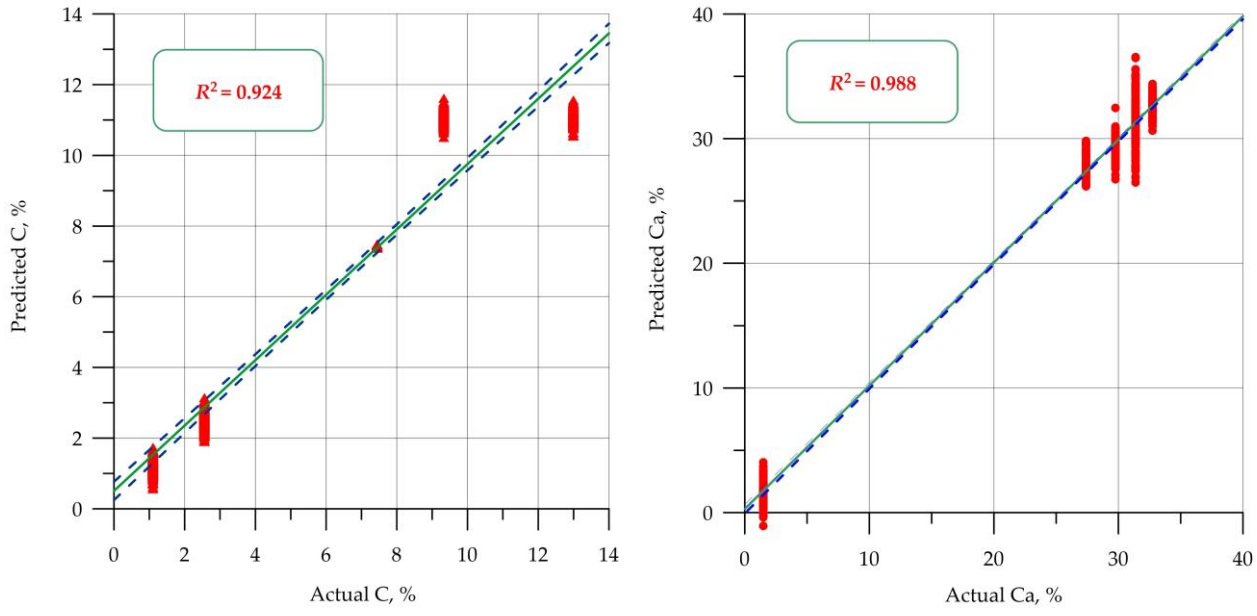

(a) (b)

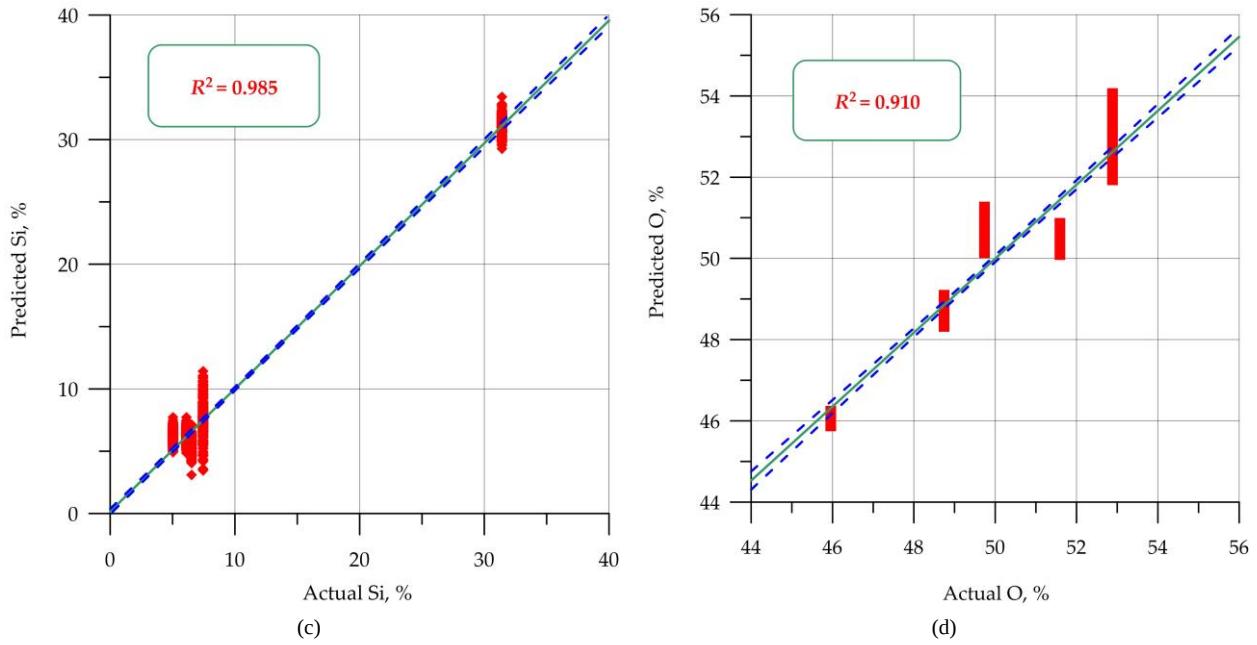

Figure 10. The comparison of experimental and predicted values: (a) for carbon C; (b) for calcium Ca; (c) for silicon Si; (d) for oxygen O

Table 8. Reliability of chemical element prediction

Element	R^2	Error, %
Ca	0.988	15
Si	0.985	9
O	0.910	11
C	0.924	18

Figures 10-a to 10-d show that all regression lines pass through the center of the diagram. This means that the estimate is unbiased. The slope of the regression line in all graphs is close to 45°, i.e. the predicted value corresponds to the actual value according to the average estimate. The general trend is stable and corresponds to the actual values within the measurement error. The regression model performs best for calcium (Ca) and silicon (Si), showing strong predictability with relatively low errors. Carbon (C) and oxygen (O) predictions show moderate accuracy, indicating that additional influencing factors such as hydration level, porosity, and weathering may need to be considered improving the model.

4. Discussion

Considering the results of the present study, mixing admixtures with composite cementitious materials may accelerate the CSH formation process in different stages or have no effect on the CSH formation process.

The results of the current study show that when GP is added to concrete, the formation of CSH is accelerated due to the increase of calcium, oxygen and carbon in EDS analysis, even the CSH crystals formed by the CSH process are obvious by SEM analysis. Adding GP admixture to concrete can induce the CSH process in concrete. According to the results, it is obvious that the formation of CSH is mostly affected in the second phase of CSH formation process. In this phase, CSH crystals are formed and the chemical elements are changed. When MS, SCG and PS were added into the composite cementitious materials, microsilica caused the development of silicon and played a major role in accelerating the formation of CSH (EDS analysis results), therefore, the SEM image results showed that when microsilica was added into the composite cementitious materials, the CSH crystals began to grow. The EDS results illustrated that when SCG was added into the composite cementitious materials, the percentage of oxygen and carbon increased, although this situation is the reason for accelerating the formation of CSH, but this process is likely to fill the voids in the third phase of CSH formation process. Moreover, mixing PS has no positive effect on the acceleration of CSH according to the EDS results.

In general, microsilica formed the CSH process in the first and second phases. The summary of the EDS and SEM results on the addition of microsilica into the composite cementitious materials illustrates that the main reason for the formation of crystals in these samples is the addition of microsilica. SCG plays the role of filler in the formation of CSH and accelerates the process of CSH by increasing the chemical elements of carbon and oxygen. PS has no effect on accelerating the formation of CSH, and the crystallization is caused by the addition of microsilica, as shown by the SEM

results. In the third sample, when MS was added to the composite cementitious materials (sandy soil), the formation process of CSH was accelerated. Meanwhile, in the third sample, the ratio of cement and water was smaller than other samples. According to the results of SEM and EDS, the needles formed the crystals of CSH, moreover, the chemical properties showed that the percentage of silica increased by less than 5%. The effect of water on MS is obvious from the convergence of the results of EDS and SEM. When the ratio of MS, cement and water was less than the optimum percentage, CSH played the role of filler and needle instead of changing the chemical properties and crystallinity. In general, when the chemical elements Silicon and Calcium increased the formation of CSH in the first phase, such as the formation of CSH gel was improved, also the second phase occurred with the results of crystallization, when Carbon and Oxygen increased the formation of CSH in the second phase, while they had the greatest influence.

In the third stage, the formation of CSH is the formation of CSH as a filling of voids. Considering other studies, the formation aspect of CSH crystallization and chemical properties occurred due to different reasons. Like Scrivener et al. [16], the nucleation theory is most restrained in finding the acceleration of CSH due to the change of chemical composition elements, while the boundary nucleation and growth (BNG) theory presented by Avrami [23] was not masked. In this study, sometimes the depth of voids depends on the presence of water and cement [50]. Ragalwar et al. [59] realized that the microsilica-cement water interface is the void filling aspect in the CSH formation process which is related to the third process of CSH while Hanpongpun et al. [26] believed that the void depth and size are related to the growth of CSH crystals, this idea was correct in some places but when GP was added to concrete it was not acceptable based on the SEM analysis results. This study opinion is close to the opinion of Oey et al. [63] since the void filling by microsilica in the CSH formation process. In another analysis, Kumar [46] found that most of the CSH crystals were less than 10 nm in size while according to the current study result, most of the CSH crystals were less than 10 µm in size unless the 10 nm CSH crystals were formed in the first phase of CSH. Overall, on the one hand, this study proved that some materials can be effective in the process of CSH formation in the first or second phase, that is, the change changes the chemical properties or crystallization occurs. Furthermore, the formation of CSH acts as a void filler in the third phase. On the other hand, this study proved that the SEM and EDS analysis can be completed together as the identification of the CSH process in different phases, which has not been done, for example, in the works that studied the microstructural transformation in cementitious materials in detail [37, 39, 40].

5. Conclusion

This study presents a comprehensive investigation of the role of different admixtures in accelerating the formation of calcium silicate hydrate (CSH) in cementitious materials. By integrating scanning electron microscopy (SEM) and energy dispersive X-ray spectroscopy (EDS), the study confirms the structural and chemical transformations induced by different types of admixtures. The results confirm that gelatin powder (GP) significantly enhances CSH formation by increasing the availability of calcium and oxygen, while microsilica (MS) promotes silicon enrichment, leading to enhanced pozzolanic reactions. However, coffee grounds (SCG) and peanut shells (PS) have limited direct effects on CSH nucleation. Moreover, SCG acts more as a filler than as an accelerator of the hydration process. Introducing a regression-based predictive model further strengthens the study by quantifying the changes in chemical composition in response to the addition of admixtures. The R^2 model estimates confirm the robustness of the predictions, particularly for calcium (Ca) and carbon (C), while identifying additional factors influencing oxygen (O) variability due to hydration and environmental influences. It should be noted that minor environmental fluctuations during curing, such as variations in temperature and humidity, could partially contribute to the variability observed in the oxygen content measured by EDS.

This predictive approach provides a new analytical framework for optimizing additive selection in cementitious composites, thereby enhancing mechanical strength, durability, and stability. By addressing gaps in previous research, particularly the lack of combined SEM-EDS structural analysis and predictive modeling, this study establishes a more comprehensive, quantitative, and actionable understanding of the mechanisms of CSH formation. The results contribute to the development of more efficient and sustainable cementitious materials, delivering improved performance in construction and infrastructure applications.

6. Declarations

6.1. Author Contributions

Conceptualization, M.H., S.A.S., and E.M.S.; methodology, M.H. and M.K.; software, M.H. and O.A.; validation, M.H.; formal analysis, M.H.; investigation, M.H., S.A.S., E.M.S., A.N.B., M.K., and O.A.; resources, M.H.; data curation, M.K.; writing—original draft preparation, S.A.S., E.M.S., M.H., and A.N.B.; writing—review and editing, S.A.S., E.M.S., M.H., and A.N.B.; visualization, M.H. and A.N.B.; supervision, A.N.B.; project administration, A.N.B.; funding acquisition, O.A. and E.M.S. All authors have read and agreed to the published version of the manuscript.

6.2. Data Availability Statement

The data presented in this study are available in the article.

6.3. Funding

The authors received no financial support for the research, authorship, and/or publication of this article.

6.4. Acknowledgements

The authors would like to acknowledge the administration of Don State Technical University for their resources.

6.5. Conflicts of Interest

The authors declare no conflict of interest.

7. References

[1] Harrisson, A. M. (2019). Constitution and specification of Portland cement. Lea's Chemistry of Cement and Concrete, Butterworth-Heinemann, Oxford, United Kingdom. doi:10.1016/B978-0-08-100773-0.00004-6.

[2] Vijayan, D. S., Devarajan, P., & Sivasuriyan, A. (2023). A review on eminent application and performance of nano based silica and silica fume in the cement concrete. Sustainable Energy Technologies and Assessments, 56, 56. doi:10.1016/j.seta.2023.103105.

[3] Raza, S. S., Amir, M. T., Azab, M., Ali, B., Abdallah, M., El Ouni, M. H., & Elhag, A. B. (2022). Effect of micro-silica on the physical, tensile, and load-deflection characteristics of micro fiber-reinforced high-performance concrete (HPC). Case Studies in Construction Materials, 17, 17. doi:10.1016/j.cscm.2022.e01380.

[4] Zhang, L., Bian, M., Xiao, Z., Wang, X., & Han, B. (2023). A comprehensive review of cementitious composites modified with nano silica: Fabrication, microstructures, properties and applications. Construction and Building Materials, 409, 409. doi:10.1016/j.conbuildmat.2023.133922.

[5] Tabish, M., Zaheer, M. M., & Baqi, A. (2023). Effect of nano-silica on mechanical, microstructural and durability properties of cement-based materials: A review. Journal of Building Engineering, 65, 65. doi:10.1016/j.jobe.2022.105676.

[6] Mohana, R., & Bavithra, K. (2023). Influence of nano materials on the macro and micro structural behaviour of high performance concrete using interfacial transition zone approach. Construction and Building Materials, 397, 397. doi:10.1016/j.conbuildmat.2023.132465.

[7] Xia, W., Cui, S. A., Zhu, L. X., Li, W. K., Ju, J. W. W., & Wang, X. W. (2023). Effects of nano-silica modification on early age hydration process in winter construction of tunnel engineering. Construction and Building Materials, 408, 133804. doi:10.1016/j.conbuildmat.2023.133804.

[8] Vipulanandan, C., & Mohammed, A. (2019). Smart cement compressive piezoresistive, stress-strain, and strength behavior with nanosilica modification. Journal of Testing and Evaluation, 47(2), 1479–1501. doi:10.1520/JTE20170105.

[9] Mohammed, A. S. (2018). Vipulanandan models to predict the electrical resistivity, rheological properties and compressive stress-strain behavior of oil well cement modified with silica nanoparticles. Egyptian Journal of Petroleum, 27(4), 1265–1273. doi:10.1016/j.ejpe.2018.07.001.

[10] Rupasinghe, M., San Nicolas, R., Mendis, P., Sofi, M., & Ngo, T. (2017). Investigation of strength and hydration characteristics in nano-silica incorporated cement paste. Cement and Concrete Composites, 80, 17–30. doi:10.1016/j.cemconcomp.2017.02.011.

[11] Jo, B. W., Kim, C. H., Tae, G. ho, & Park, J. Bin. (2007). Characteristics of cement mortar with nano-SiO2 particles. Construction and Building Materials, 21(6), 1351–1355. doi:10.1016/j.conbuildmat.2005.12.020.

[12] Babu, G. R., Ramana, N. V., Kumar, T. N., & Kumar, K. V. (2019). Effect of nanosilica on properties and durability in cement. Materials Today: Proceedings, 19, 599-605. doi:10.1016/j.matpr.2019.07.739.

[13] Singh, L. P., Ali, D., & Sharma, U. (2016). Studies on optimization of silica nanoparticles dosage in cementitious system. Cement and Concrete Composites, 70, 60–68. doi:10.1016/j.cemconcomp.2016.03.006.

[14] Zhang, A., Ge, Y., Yang, W., Cai, X., & Du, Y. (2019). Comparative study on the effects of nano-SiO2, nano-Fe2O3 and nano-NiO on hydration and microscopic properties of white cement. Construction and Building Materials, 228, 116767. doi:10.1016/j.conbuildmat.2019.116767.

[15] Nguyen, V. T., Lee, S. Y., Chung, S. Y., Moon, J. H., & Kim, D. J. (2023). Use of multiphase voxels to simulate the effects of nano-silica on cement hydration. Case Studies in Construction Materials, 18, 1909. doi:10.1016/j.cscm.2023.e01909.

[16] Scrivener, K., Ouzia, A., Juilland, P., & Kunhi Mohamed, A. (2019). Advances in understanding cement hydration mechanisms. Cement and Concrete Research, 124, 1058. doi:10.1016/j.cemconres.2019.105823.

[17] Sowoidnich, T., Bellmann, F., Damidot, D., & Ludwig, H. M. (2019). New insights into tricalcium silicate hydration in paste. Journal of the American Ceramic Society, 102(5), 2965–2976. doi:10.1111/jace.16133.

[18] Barkatt, A., Macedo, P. B., Gibson, B. C., & Montrose, C. J. (1984). Modelling of Waste Form Performance and System Release. MRS Proceedings, 44. doi:10.1557/proc-44-3.

[19] Nicoleau, L., Nonat, A., & Perrey, D. (2013). The di- and tricalcium silicate dissolutions. Cement and Concrete Research, 47, 14–30. doi:10.1016/j.cemconres.2013.01.017.

[20] Gislason, S. R., & Oelkers, E. H. (2003). Mechanism, rates, and consequences of basaltic glass dissolution: II. An experimental study of the dissolution rates of basaltic glass as a function of pH and temperature. Geochimica et Cosmochimica Acta, 67(20), 3817–3832. doi:10.1016/S0016-7037(00)00176-5.

[21] Avrami, M. (1939). Kinetics of phase change. I: General theory. The Journal of Chemical Physics, 7(12), 1103–1112. doi:10.1063/1.1750380.

[22] Rukzon, S., Rungruang, S., Thepwong, R., Chaisakulkiet, U., & Chindaprasirt, P. (2024). Optimizing Mortar Mixtures with Basalt Rubble: Impacts on Compressive Strength and Chloride Penetration. Civil Engineering Journal (Iran), 10(12), 4008–4018. doi:10.28991/CEJ-2024-010-12-013.

[23] Andalibi, M. R., Kumar, A., Srinivasan, B., Bowen, P., Scrivener, K., Ludwig, C., & Testino, A. (2018). On the mesoscale mechanism of synthetic calcium-silicate-hydrate precipitation: A population balance modeling approach. Journal of Materials Chemistry A, 6(2), 363–373. doi:10.1039/c7ta08784e.

[24] Ouzia, A. R. C. W. C. (2019). Modeling the kinetics of the main peak and later age of alite hydration. EPFL, 263. doi:10.5075/epfl-thesis-9499.

[25] Avet, F., & Scrivener, K. (2018). Investigation of the calcined kaolinite content on the hydration of Limestone Calcined Clay Cement (LC3). Cement and Concrete Research, 107, 124–135. doi:10.1016/j.cemconres.2018.02.016.

[26] Hanpongpun, W. (2019). Investigation of the use of Limestone Calcined Clay Cement (LC3) applied to Thailand. EPFL-Lausanne, 4. doi:10.5075/epflthesis-9005.

[27] Zhang, L., Jing, H., Gao, Y., Yu, Z., & Liu, Y. (2024). Enhancement of the tensile properties of cement mortar composites with nanoadditives produced by chemical vapor deposition. Case Studies in Construction Materials, 21, 3469. doi:10.1016/j.cscm.2024.e03469.

[28] González-Coneo, J., Zarzuela, R., Luna, M., & Mosquera, M. J. (2024). Water-soluble fluorosilane supplemented with fumed silica as admixture for producing hydrophobic concrete: Effects on cement hydration, mechanical properties and water protection properties. Developments in the Built Environment, 17, 100317. doi:10.1016/j.dibe.2023.100317.

[29] Al-kroom, H., Rashad, A. M., Alghamdi, H., Abadel, A. A., Elrahman, M. A., Abdel-Gawwad, H. A., & Arif, M. A. (2024). Application of pretreated dealuminated kaolin as a modifier agent for alkali-activated slag cement. Case Studies in Construction Materials, 20. doi:10.1016/j.cscm.2024.e02858.

[30] Ijaz, N., Ye, W. M., Rehman, Z. ur, Ijaz, Z., & Junaid, M. F. (2024). Global insights into micro-macro mechanisms and environmental implications of limestone calcined clay cement (LC3) for sustainable construction applications. Science of the Total Environment, 907, 167794. doi:10.1016/j.scitotenv.2023.167794.

[31] Chiadighikaobi, P. C., Hasanzadeh, A., Hematibahar, M., Kharun, M., Mousavi, M. S., Stashevskaya, N. A., & Adegoke, M. A. (2024). Evaluation of the mechanical behavior of high-performance concrete (HPC) reinforced with 3D-Printed trusses. Results in Engineering, 22. doi:10.1016/j.rineng.2024.102058.

[32] Hematibahar, M., Hasanzadeh, A., Kharun, M., Beskopylny, A. N., Stel'makh, S. A., & Shcherban', E. M. (2024). The Influence of Three-Dimensionally Printed Polymer Materials as Trusses and Shell Structures on the Mechanical Properties and Load-Bearing Capacity of Reinforced Concrete. Materials, 17(14), 17. doi:10.3390/ma17143413.

[33] Saprykina, T. K., & Zhadanov, V. I. (2025). Improving Theoretical Concepts of Composition Design of Dispersedly-Reinforced Concretes. Modern Trends in Construction, Urban and Territorial Planning, 3(4), 66–73. doi:10.23947/2949-1835-2024-3-4-66-73.

[34] Shcherban', E. M., Stel'makh, S. A., Beskopylny, A. N., Mailyan, L. R., Meskhi, B., Chernil'nik, A., El'shaeva, D., Pogrebnyak, A., & Yaschenko, R. (2024). Influence of Sunflower Seed Husks Ash on the Structure Formation and Properties of Cement Concrete. Civil Engineering Journal (Iran), 10(5), 1475–1493. doi:10.28991/CEJ-2024-010-05-08.

[35] Shu, Y., & Zhang, J. (2023). Effect of Basalt Fiber Content and Length on the Strength and Crack Development of Polyvinyl Alcohol/Basalt Hybrid Fiber-Reinforced Cement Soil. Polymers, 15(9), 2146. doi:10.3390/polym15092146.

[36] Hematibahar, M., Kharun, M., Beskopylny, A. N., Stel'makh, S. A., Shcherban', E. M., & Razveeva, I. (2024). Analysis of Models to Predict Mechanical Properties of High-Performance and Ultra-High-Performance Concrete Using Machine Learning. Journal of Composites Science, 8(8), 287. doi:10.3390/jcs8080287.

[37] Gou, J., Li, S., Jiang, C., Li, Z., & You, G. (2025). A Study on the Influence of Gypsum and Ca(OH)2 on the Mechanical Properties and Hydration Behavior of Multi-Component Solid Waste-Based Cementitious Materials. Materials, 18(9), 18. doi:10.3390/ma18091964.

[38] Jiang, L., Zhao, X., & Wang, H. (2025). Synthesis and Property Characterization of Low-Activity Waste-Derived Quaternary Cementitious Materials. Buildings, 15(9), 15. doi:10.3390/buildings15091426.

[39] Chen, J., Yu, K., Li, S., & Liu, D. (2025). Exploring the Mechanism of Microstructural Changes in Ultra-High-Performance Concrete Under Microwave Influence: Experiments and Molecular Dynamics Simulation. Materials, 18(9), 18. doi:10.3390/ma18091892.

[40] Yu, L., Xu, X., Ni, S., Meng, D., Meng, X., & Xu, B. (2025). Experimental and Molecular Dynamics Simulation Study on Sulfate Corrosion Resistance of Cellulose-Nanocrystal-Modified ECC. Applied Sciences (Switzerland), 15(6), 3205. doi:10.3390/app15063205.

[41] Buettner, N., Iyacu, G., Dal Poggetto, G., & Akono, A. T. (2025). The Effect of Carbon Nanofibers on the Microstructure, Chemistry, and Pore Structure of Concrete Made with Fine Recycled Concrete Aggregates. Nanomaterials, 15(4), 253. doi:10.3390/nano15040253.

[42] Lam, T. Van, & Nguyen, M. H. (2023). Incorporating Industrial By-Products into Geopolymer Mortar: Effects on Strength and Durability. Materials, 16(12), 4406. doi:10.3390/ma16124406.

[43] Alam, S., & Alselami, N. A. (2024). Geotechnical Properties of Fly Ash Blended Expansive Soil: A Review. Civil Engineering Journal, 10, 82–103. doi:10.28991/cej-sp2024-010-06.

[44] Bigi, A., Bracci, B., & Panzavolta, S. (2004). Effect of added gelatin on the properties of calcium phosphate cement. Biomaterials, 25(14), 2893–2899. doi:10.1016/j.biomaterials.2003.09.059.

[45] Alaj, A., Krasniqi, N., & Numao, T. (2024). Effect of Non-Class Fly Ash on Strength Properties of Concrete. Civil Engineering Journal (Iran), 10(3), 689–698. doi:10.28991/CEJ-2024-010-03-02.

[46] Kumar, A. (2017). Synthetic Calcium Silicate Hydrates. PhD Thesis, Swiss Federal Technology Institute of Lausanne, Lausanne, Switzerland.

[47] Kaya, M. (2020). Evaluating organic waste sources (spent coffee ground) as metal-free catalyst for hydrogen generation by the methanolysis of sodium borohydride. International Journal of Hydrogen Energy, 45(23), 12743–12754. doi:10.1016/j.ijhydene.2019.10.180.

[48] Suksiripattanapong, C., Kua, T. A., Arulrajah, A., Maghool, F., & Horpibulsuk, S. (2017). Strength and microstructure properties of spent coffee grounds stabilized with rice husk ash and slag geopolymers. Construction and Building Materials, 146, 312–320. doi:10.1016/j.conbuildmat.2017.04.103.

[49] Ballesteros, L. F., Teixeira, J. A., & Mussatto, S. I. (2014). Chemical, Functional, and Structural Properties of Spent Coffee Grounds and Coffee Silverskin. Food and Bioprocess Technology, 7(12), 3493–3503. doi:10.1007/s11947-014-1349-z.

[50] Bizzozero, J., Gosselin, C., & Scrivener, K. L. (2014). Expansion mechanisms in calcium aluminate and sulfoaluminate systems with calcium sulfate. Cement and Concrete Research, 56, 190–202. doi:10.1016/j.cemconres.2013.11.011.

[51] Yu, C., Sun, W., & Scrivener, K. (2013). Mechanism of expansion of mortars immersed in sodium sulfate solutions. Cement and Concrete Research, 43(1), 105–111. doi:10.1016/j.cemconres.2012.10.001.

[52] Bazzoni, A. (2014). Study of early hydration mechanisms of cement by means of electron microscopy. Ph.D. Thesis, Swiss Federal Technology Institute of Lausanne, Lausanne, Switzerland.

[53] Qu, Z., Yu, Q., Ong, G. P., Cardinaels, R., Ke, L., Long, Y., & Geng, G. (2023). 3D printing concrete containing thermal responsive gelatin: Towards cold environment applications. Cement and Concrete Composites, 140, 105029. doi:10.1016/j.cemconcomp.2023.105029.

[54] Wang, Y., Lu, H., Wang, J., & He, H. (2020). Effects of highly crystalized nano C-S-H particles on performances of portland cement paste and its mechanism. Crystals, 10(9), 1–17. doi:10.3390/cryst10090816.

[55] Wang, Q., Li, S., Wang, J., Pan, S., Lv, C., Cui, X., & Guo, Z. (2018). Effect of Graphene Oxide on Hydration Process and Main Hydration Products of Cement. Kuei Suan Jen Hsueh Pao/Journal of the Chinese Ceramic Society, 46(2), 163–172. doi:10.14062/j.issn.0454-5648.2018.02.10.

[56] Berenguer, R., Lima, N., Pinto, L., Monteiro, E., Povoas, Y., Oliveira, R., & Lima, N. B. D. (2021). Cement-based materials: Pozzolanic activities of mineral additions are compromised by the presence of reactive oxides. Journal of Building Engineering, 41, 102358. doi:10.1016/j.jobe.2021.102358.

[57] Gartner, E., Maruyama, I., & Chen, J. (2017). A new model for the CSH phase formed during the hydration of Portland cements. Cement and Concrete Research, 97, 95-106. doi:10.1016/j.cemconres.2017.03.001.

[58] Yee, J. J., Khong, S. C., Tee, K. F., Jolius, G., & Chin, S. C. (2024). Spent coffee grounds enhanced compressive strength of cement mortar: an optimization study. Discover Applied Sciences, 6(7), 379. doi:10.1007/s42452-024-06077-9.

[59] Ragalwar, K., Heard, W. F., Williams, B. A., & Ranade, R. (2020). Significance of the particle size distribution modulus for strain-hardening-ultra-high performance concrete (SH-UHPC) matrix design. Construction and Building Materials, 234, 117423. doi:10.1016/j.conbuildmat.2019.117423.

[60] Gupta, S., & Kashani, A. (2021). Utilization of biochar from unwashed peanut shell in cementitious building materials – Effect on early age properties and environmental benefits. Fuel Processing Technology, 218. doi:10.1016/j.fuproc.2021.106841.

[61] Pandey, L., Sarkar, S., Arya, A., Sharma, A. L., Panwar, A., Kotnala, R. K., & Gaur, A. (2023). Fabrication of activated carbon electrodes derived from peanut shell for high-performance supercapacitors. Biomass Conversion and Biorefinery, 13(8), 6737–6746. doi:10.1007/s13399-021-01701-9.

[62] Lima, N. B., Junior, R. V. A., Belarmino, M. K. D. L., Estolano, A. M. L., Manta, R. C., Teti, B. S., Júnior, B. B., Póvoas, Y. V., Monteiro, E. C. B., Oliveira, R. A., & Lima, N. B. D. (2019). Loss of mass, structural, and thermodynamic properties of concretes under rainy conditions. Journal of Molecular Structure, 1176, 622–632. doi:10.1016/j.molstruc.2018.09.006.

[63] Oey, T., Kumar, A., Bullard, J. W., Neithalath, N., & Sant, G. (2013). The filler effect: The influence of filler content and surface area on cementitious reaction rates. Journal of the American Ceramic Society, 96(6), 1978–1990. doi:10.1111/jace.12264.

[64] Puzatova, A. V., Dmitrieva, M. A., Tovpinets, A. O., & Leitsin, V. V. (2024). Study of Structural Defects Evolution in Fine-Grained Concrete Using Computed Tomography Methods. Advanced Engineering Research (Rostov-on-Don), 24(3), 227–237. doi:10.23947/2687-1653-2024-24-3-227-237.